

The random Blume-Capel model on cubic lattice: first order inverse freezing in a 3D spin-glass system

L. Leuzzi,^{1,2,*} M. Paoluzzi,^{1,3} and A. Crisanti²

¹*IPCF-CNR, UOS Roma, P.le Aldo Moro 2, I-00185 Roma, Italy*

²*Dipartimento di Fisica, Università "Sapienza", P.le Aldo Moro 2, I-00185 Roma, Italy*

³*Dipartimento di Fisica, Università di Roma 3, Via della Vasca Navale 84, I-00146 Roma, Italy*

(Dated: November 9, 2018)

We present a numerical study of the Blume-Capel model with quenched disorder in 3D. The phase diagram is characterized by spin-glass/paramagnet phase transitions of both first and second order in the thermodynamic sense. Numerical simulations are performed using the Exchange-Monte Carlo algorithm, providing clear evidence for inverse freezing. The main features at criticality and in the phase coexistence region are investigated. The whole inverse freezing transition appears to be first order. The second order transition appears to be in the same universality class of the Edwards-Anderson model. The nature of the spin-glass phase is analyzed by means of the finite size scaling behavior of the overlap distribution functions and the four-spins real-space correlation functions. Evidence for a replica symmetry breaking-like organization of states is provided.

PACS numbers:

I. INTRODUCTION

The so-called *inverse transition* (IT) is a reversible transformation occurring between phases whose entropic contents and symmetries are in the inverse order relation relatively to standard transitions. The case - already hypothesized by Tammann more than a century ago¹ - of "ordering in disorder" taking place in a crystal solid that liquefies on cooling, is generally termed *inverse melting*. The IT phenomenon also includes the transformation involving amorphous solid phases - rather than crystal - as that of a liquid vitrifying upon heating. In this case the term *inverse freezing* is somewhat used in the literature: both phases are disordered but the fluid appears to be the one with least entropic content. The reason for these counter intuitive phenomena is that a phase usually present only at high temperature happens to exist also in peculiar patterns such that its entropy is actually less than the one of the phase normally considered the most ordered one.

Inverse transitions in their most generic meaning (i.e., both thermodynamic or occurring by means of kinetic arrest) have been detected in the last years in a number of different materials and between phases of rather different nature. The first example was the transition between liquid and crystal phases of helium isotopes He³ and He⁴ at low temperature.² A more complex and recent example is the polymer poly(4-methylpentene-1) - P4MP1 - in which a crystal polymer melts as the temperature is decreased, or the pressure increased. By means of exhaustive measurements by Differential Scanning Calorimetry (DSC) and X-ray diffraction the phase diagram of P4MP1 has been experimentally determined by the group of Rastogi,³⁻⁵ showing evidence for both an equilibrium inverse melting, between a crystal phase (tetragonal or hexagonal, depending on the pressure) and a fluid phase, and a non-equilibrium IT between the hexagonal crystal and a glassy phase. Another extensively

studied instance is a molecular solution in water, composed by α -cyclodextrine (α CD) and 4-methylpyridine (4MP) mixed in given molecular ratios, investigated by means of neutron scattering, X-ray diffraction, DSC and rheometric measurements.⁶⁻¹⁵ The "solid" is in this case a sol-gel porous system formed by an ordered network of molecules of α CD-water-4MP filled with liquid 4MP, melting down decreasing temperature at constant α CD concentration. Eventually, another important polymeric example is methyl-cellulose solution in water, undergoing a reversible inverse sol-gel transition.^{16,17} For such system, a careful analysis of the behavior of the microscopic components across the transition has been performed in literature¹⁸ and, therefore, it turns out to be particularly important for the modelization proposed in the present work, as we will see in the following.

Apart from polymeric and macromolecular substances, in the last years ITs showed up in many other different contexts. Inverse melting from an ordered lattice to a disordered vortex phase takes place, e.g., for the magnetic flux lines in a high temperature superconductor.¹⁹ A gas of atoms at zero temperature passes from superfluid to insulator as the lattice potential depth is increased.²⁰ Furthermore, in the framework of nanosystems, the reversible transition of an isotropic liquid into an ordered cubic phase upon heating has been detected experimentally in ferromagnetic systems of gold nanoparticles.^{21,22}

In this work we stick to a definition of IT as the one put forward by Tammann:¹ a reversible transition in temperature at fixed pressure - or generally speaking, at a fixed parameter *externally* tuning the interaction strength, such as concentration, chemical potential or magnetic field - from a solid high temperature phase to an isotropic fluid (or a paramagnet, for magnetic systems) low temperature phase. Generalizing to non-equilibrium systems one might address as IT also those cases in which the isotropic fluid is dynamically arrested into a glassy state. This occurs, e.g., for the crystal-glass transition

in the cited P4MP1 as pressure is not too large³ or in molecular dynamics simulations and mode-coupling computations of attractive colloidal glasses.^{23,24}

In this definition IT is not an exact synonym of reentrance. Indeed, though a reentrance in the transition line is a common feature in ITs, this is not always present, as, e.g., in the case of α CD^{6,7,10} or methyl-cellulose¹⁶ solutions for which no high temperature fluid phase has been detected. Moreover, not all re-entrances can be seen as signatures of an IT to a completely disordered isotropic phase. In liquid crystals, ultra-thin films and other materials, phases with different kind of symmetry can, actually, be found that are separated by reentrant isobaric transition lines in temperature - cf., e.g., Refs. [25–29] - but no melting occurs *strictu sensu*. Also re-entrances between dynamically arrested states, aperiodic structures or amorphous solids of qualitatively similar nature, like liquid-liquid pairs^{30,31} are not considered as IT, since an a-priori order relationship between the entropic content of the two phases is not established and it cannot be claimed what is inverse and what is "standard". For the same reasons also re-entrances between spin-glass (supposed at *equilibrium*, that is, considered as a thermodynamic phase) and ferromagnetic phases - as, e.g., in Refs. [32,33] - hardly fall into the IT category. Eventually, re-entrances in parameters other than temperature are also not taken into account as inverse melting/freezing transitions.

A thorough explanation of the fundamental mechanisms leading to the IT would need of a microscopic analysis of the single components behavior and their mutual interactions as temperature changes across the critical point. Due to the complexity of the structure of polymeric chains and macromolecules involved in such transformations, a clear-cut picture of the state of the single components is often not available. For the case of the above mentioned methyl-cellulose, Haque and Morris¹⁸ proposed that chains exist in solution as folded bundles in which hydrophobic methyl groups are packed. As the temperature is raised, the bundles unfold, exposing methyl groups to water molecules and, thus, causing a large increase in volume and the formation of hydrophobic links eventually leading to a gel. The polymers in the folded state are thus inactive (or far less interacting than those in the unfolded state) but also yield a smaller entropic contribution than the unfolded ones. As the chains start to unfold because of thermal noise they change to an interacting state thus enforcing bonds with other chains and condensing in a gel.

Theoretical modeling for IT is starting to develop but is still on its first, often uncorrelated, steps and consists, at the better, in heuristic reproductions of the phenomenon.^{34–41} Looking, in particular, at the transition between an amorphous 'frozen' phase and a fluid (i.e., paramagnet), recently spin-glass models with spin-1 variables have turned out to effectively represent systems in which the transformation is driven by entropic effects. In these cases inverse freezing has been studied in the

mean-field approximation.^{40,41}

We also mention that with the help of this class of models, the connection between entropy driven phase reentrance and shear *thickening* can also be tackled⁴² and, furthermore, a generalization of the spin-1 variable to a composition of "fast" and "slow" variables⁸⁴ coupled to two different thermal baths allows for studying anomalous latent heat in out of equilibrium transitions.⁴³

In the present work we will consider the Blume-Capel (BC) model⁴⁴ with quenched disorder: a spin-glass model on a 3D cubic lattice with bosonic spin-1 variables ($s_i = -1, 0, +1$). Under the assumption that the interplay between inactive and interactive states of a microscopic component is at the ground of the eventual IT, bosonic spins can approximate the folded/unfolded conformation, $S = 0$ representing the inactive state, $S = \pm 1$ the interactive one, cf. Ref. [38] for a more comprehensive discussion. We will focus on the random version of the BC model introduced by Ghatak and Sherrington⁴⁵ (GS) in order to study the effects of the crystal-field in a spin glass - e.g., $(\text{Ti}_{1-x}\text{V}_x)_2\text{O}_3$ displays anisotropic spin glass behavior in function of x .⁴⁶ The mean-field solution in the Full Replica Symmetry Breaking (RSB) scheme^{40,47–49} predicts a phase diagram with a second order transition line between spin-glass (SG) and paramagnetic (PM) phase ending in a tricritical point where a first order phase transition line starts and a phase coexistence region appears.⁸⁵ Furthermore, the first order transition is characterized by the phenomenon of IT:^{40,49} the low temperature phase is PM with a lower entropy than the SG phase and the transition line develops a reentrance.

In the original (ferromagnetic) BC models^{44,50} however, no IT was observed in the mean-field approximation, nor in finite dimension studies.^{51–54} and in presence of quenched disorder a recent study on a 3D hierarchical lattice by means of renormalization group theory in position space⁵⁵ provides no evidence for a low temperature tricritical point or a PM/SG reentrance, contrarily to what is predicted by mean-field theory.

Moreover, we found in the literature only one finite dimensional system with quenched disorder undergoing a standard first order phase transition in finite dimension: the 4-Potts glass studied by Fernandez *et al.* in Ref. [56]. In that work a first claim has been made that first order phase transition exists in 3D systems also in presence of quenched disorder, though the randomness tends to strongly smoothen the transition into a second order one. This transition is driven by the temperature and by the degree of dilution of the Potts glass bonds. Though in numerical simulations changing, e.g., the pressure, the bond dilution, or even the relative probabilities of the random bond values, cf., e.g., Ref. [57], is technically equivalent, the latter are complicated to control in a real experiment and require the preparation of several samples with different microscopic properties. The study of a conceptually simpler model, satisfactorily approachable with standard simulation techniques, might help in

validating the assessment of the existence of first order phase transitions in random systems.

Motivated by the above considerations we have, thus, studied the existence of inverse freezing in the 3D disordered BC model with nearest-neighbor interactions and the nature of the “frozen” (or, rather, “blocked”) phase. We present hereafter the results of our investigation by means of Monte Carlo numerical simulations. Some results about the critical behavior have already appeared in a recent letter.⁵⁸

In the present manuscript we first introduce the model, in Sec. II, and in Secs. III and IV we define the numerical techniques employed to study continuous and discontinuous phase transitions in finite size (FS) systems. In Sec. V we recall the Exchange Monte Carlo method, else called Parallel Tempering (PT).^{59,60} In Sec. VI, we present our results about the phase diagram of the model and its critical behavior both along the continuous transition and in the coexistence region related to the first order transition. The main features of the organization of states in the SG phase in finite dimension (i.e., below the upper critical dimension for our model) is studied in Sec. VII, where we perform a systematic study of the properties of the overlap distribution functions and of the four-spins correlation functions in space. Finally, Sec. VIII reports our conclusions.

II. MODEL AND ORDER PARAMETERS

We consider the following Hamiltonian

$$\mathcal{H}_J[s] = - \sum_{(ij)} J_{ij} s_i s_j + D \sum_i s_i^2 \quad (1)$$

where (ij) indicates ordered couples of nearest-neighbor sites, and $s_i = -1, 0, +1$ are spin-1 variables lying on a cubic lattice of size $N = L^3$ with Periodic Boundary Condition (PBC). Random couplings J_{ij} are independent identically distributed as

$$P(J_{ij}) = \frac{1}{2} \delta(J_{ij} - 1) + \frac{1}{2} \delta(J_{ij} + 1) \quad (2)$$

The field D is usually called crystal-field and it plays the role of a chemical potential for the empty sites $s = 0$. We will, therefore, refer to D invariably as chemical potential or crystal field in the following. We simulate two real replicas of the system and define their site and link overlaps, i.e., the order parameters usually characterizing the SG transition, as

$$q_s^{(J)} \equiv \frac{1}{N} \sum_i s_i^{(1)} s_i^{(2)} \quad (3)$$

$$q_l^{(J)} \equiv \frac{1}{3N} \sum_{(jk)} s_j^{(1)} s_k^{(1)} s_j^{(2)} s_k^{(2)} \quad (4)$$

where 3 is the dimension of the space. If a thermodynamic phase transition occurs, with latent heat, the most

significant order parameter that drives the transition is the density ρ of magnetically active ($|s_i| = 1$) sites:

$$\rho^{(J)} = \frac{1}{N} \sum_i s_i^2 \quad (5)$$

The apex J recalls us that the values of the parameters depend on the particular realization of disorder ($\{J_{ij}\}$). Useful information about the equilibrium properties of the system can be obtained from the knowledge of the following probability distribution functions (pdf)

$$P(q_s) \equiv \overline{P_J(q_s)} = \overline{\langle \delta(q_s - q_s^{(J)}) \rangle} \quad (6)$$

$$P(q_l) \equiv \overline{P_J(q_l)} = \overline{\langle \delta(q_l - q_l^{(J)}) \rangle} \quad (7)$$

$$P(\rho) \equiv \overline{P_J(\rho)} = \overline{\langle \delta(\rho - \rho^{(J)}) \rangle} \quad (8)$$

where $\overline{\dots}$ denotes the average over quenched disorder and $\langle \dots \rangle$ the thermal average. Though the density probability distribution is known to be self-averaging ($\lim_{N \rightarrow \infty} P_{J,N}(\rho) = \overline{P_J(\rho)}$), this does not hold for the overlap distributions $P_J(q_{s,l})$,⁶¹ for which⁸⁶

$$P(q_{s,l}) \equiv \overline{P_J(q_{s,l})} \neq \lim_{N \rightarrow \infty} P_{J,N}(q_{s,l}) \quad (9)$$

Through the study of the pdfs, as function of the external thermodynamic parameters, we can identify the PM /SG transition and discriminate between first and second order phase transitions. As an instance, if a first order phase transition takes place, the density pdf $P(\rho)$ displays a double peak due to the coexistence of the PM and SG phases. Moreover, by means of the overlap pdfs we can investigate the nature of the SG phase.

III. FINITE SIZE SCALING FOR CONTINUOUS TRANSITIONS

In order to infer the details of the critical behavior from numerical simulations of finite size systems, a fundamental quantity (in zero external magnetic field) is

$$C_4(\mathbf{r}) \equiv \frac{1}{N} \sum_{\mathbf{s}} \overline{\langle s_{\mathbf{s}} s_{\mathbf{s}+\mathbf{r}} \rangle^2} \quad (10)$$

with $\mathbf{r} = (r_x, r_y, r_z)$. In terms of space-dependent overlaps, $q_{\mathbf{r}} = s_{\mathbf{r}}^{(1)} s_{\mathbf{r}}^{(2)}$, C_4 can be written as

$$\begin{aligned} C_4(\mathbf{r}) &\equiv \frac{1}{N} \sum_{\mathbf{p}} \overline{\langle q_{\mathbf{p}} q_{\mathbf{p}+\mathbf{r}} \rangle_{12}} \\ &= \frac{1}{N} \sum_{\mathbf{p}} \overline{\langle s_{\mathbf{p}}^{(1)} s_{\mathbf{p}+\mathbf{r}}^{(1)} \rangle_1 \langle s_{\mathbf{p}}^{(2)} s_{\mathbf{p}+\mathbf{r}}^{(2)} \rangle_2} \end{aligned} \quad (11)$$

where $\langle \dots \rangle_{12}$ stays equivalently for the thermal average $\langle \langle \dots \rangle_1 \rangle_2$ or $\langle \langle \dots \rangle_2 \rangle_1$ over the two replicas independently.

This is the four-spins correlation function, and the information it provides can be exploited in different ways to identify the existence of a second order phase transition for finite size systems and probe the thermodynamic behavior in the SG phase.

A conventional way to identify a second order phase transition is to look at the behavior of a correlation length-like scaling function defined as

$$\xi_c^2 \equiv \frac{\int dr r^2 C_4(r)}{\int dr C_4(r)} = \left. \frac{\partial \log \hat{C}_4(\mathbf{k})}{\partial k^2} \right|_{k^2=0} \quad (12)$$

where

$$\hat{C}_4(\mathbf{k}) = \frac{1}{(2\pi)^3} \int d^3r e^{-i\mathbf{k}\cdot\mathbf{r}} C_4(\mathbf{r}) .$$

On a 3D cubic lattice, the above defined correlation length becomes:⁶²

$$\xi_c^2 = \frac{1}{4 \sin^2 \frac{k_1}{2}} \left(\frac{\hat{C}_4(\mathbf{0})}{\hat{C}_4(\mathbf{k}_1)} - 1 \right) \quad (13)$$

where $k_1 = |\mathbf{k}_1|$, $\mathbf{k}_1 \equiv (2\pi/L, 0, 0)$ is the minimum wave-vector of the lattice and $\mathbf{0} = (0, 0, 0)$. In the thermodynamic limit, a second order transition is characterized by a diverging correlation length, at critical temperature T_c , whose Finite Size Scaling (FSS) behavior is the same as in Eq. (13).^{63,71}

Another relevant observable is the SG susceptibility

$$\chi_{SG} \equiv L^3 \overline{\langle q^2 \rangle} = L^3 \hat{C}_4(\mathbf{0}) \quad (14)$$

diverging at the PM/SG transition as $L \rightarrow \infty$. Because of FS, though, ξ_c and χ_{SG} cannot diverge in numerical simulations, although inside the critical region a remarkable property of the critical phenomena survives: scale invariance. Indeed, we can define a FS ‘‘critical’’ temperature T_c^L , function of the size L , as the temperature at which the above mentioned observables do not (or only slightly) depend on the size:

$$\frac{\xi_c}{L} = \bar{\xi}_c \left(\frac{\xi_c}{L} \right) = \bar{\xi}(L^{1/\nu}(T - T_c^L)) \quad (15)$$

$$\chi_{SG} L^{\eta-2} = \bar{\chi} \left(\frac{\xi_c}{L} \right) = \bar{\chi}(L^{1/\nu}(T - T_c^L)) \quad (16)$$

The values T_c^L at which ξ_c/L at different L cross each other are the FS respective of the critical temperature. The latter can, thus, be estimated by FSS in the $L \rightarrow \infty$ limit.

A further size independent observable at criticality is the so-called Binder parameter:

$$g(L, T) = \frac{1}{2} \left(3 - \frac{q_4}{(q_2)^2} \right) \quad (17)$$

with $q_n \equiv \overline{\langle (q_s^{(J)})^n \rangle}$. It measures the deviation of $P(q)$ from a Gaussian distribution as the SG phase is approached. Since q_4 and q_2^2 scale with L in the same way, g does not depend on L at T_c .

A. Quotient method

Denoting by $O(T, L)$ a generic observable diverging at critical temperature T_c as $L \rightarrow \infty$, and considering two sizes L, L' whose scale ratio is $s = L'/L$, we can look at the scaling of quotient

$$\frac{O(T, sL)}{O(T, L)} = F_O \left(\frac{\xi_c(L, T)}{L}, s \right) + \mathcal{O}(\xi_c^{-\omega}, L^{-\omega}) \quad (18)$$

where F_O is a universal FSS function and ω is the power of the subleading FS corrections. Through the scaling Ansatz, (18) one, thus, introduces a class of universal functions F_O that are size-independent in the critical region. Given two observables O and R displaying scale invariance, this allows for plotting F_O vs F_R for several values of L : if the data collapse in a universal scaling function, the scaling Ansatz is verified and FSS methods can be trusted to evaluate the critical exponents. We will analyze in the present manuscript the behavior of $F_\xi, F_{\chi_{SG}}$ and F_g .

In order to estimate the critical exponents we can, thus, use the so-called *quotient method*,⁷¹ based on the observation that at $T_c^L \equiv T_c^*$, the correlation lengths in systems of sizes L and sL (in L units) are equal:

$$\frac{s \xi_c(T_c^*, L)}{\xi_c(T_c^*, sL)} = 1. \quad (19)$$

For an observable O scaling as t^{x_O} ($t = T/T_c - 1$) in the thermodynamic limit, it holds:

$$s \frac{x_O}{\nu} = \frac{O(T_c^*, sL)}{O(T_c^*, L)} + \mathcal{O}(L^{-\omega}) \quad (20)$$

where the dependence through $\xi_c^{-\omega}$ in the correction term is neglected because, in the critical region, $\xi_c \gg L$. For a SG we can obtain the exponents ν and η by means of the FSS of the quotients of $\partial_\beta \xi$ and χ_{SG} , scaling, respectively, with exponents

$$\begin{aligned} x_{\partial_\beta \xi} &= 1 + \nu \\ x_{\chi_{SG}} &= (2 - \eta)\nu . \end{aligned}$$

These relations hold if the Ansatz (18) is verified,⁶² i.e., if F_O is a size-independent scaling function for several values of L and sL .

IV. CHARACTERIZATION OF A FIRST ORDER TRANSITION

Besides the second order transition, the random BC mean-field model also shows a tricritical point beyond which a true first order phase transition with non-zero latent heat occurs and from which a region of coexistence of PM and SG phase departs.⁴⁰ The slope of a first order

line is given by the Clausius-Clapeyron equation that, for our model reads

$$\frac{dD}{dT} = \frac{s_{PM} - s_{SG}}{\rho_{PM} - \rho_{SG}} = \frac{\Delta s}{\Delta \rho} \quad (21)$$

where D plays the role of the pressure. The equilibrium transition line changes slope in a point where the entropy of the two coexistence phase is equal $\Delta s = 0$ (Kauzmann locus^{34,64}).

In order to tackle the identification of a first order phase transition in a 3D finite size system from numerical simulation data we sketch in the following four methods to estimate critical (and spinodal) points.

A. “Equal weight” estimate

The transition takes place at the point at which the configurations belonging to the SG phase and those belonging to the PM phase have the same statistical weight, i.e., they yield identical contribution to the partition function of the single pure phase. Else said, the free energies of the two coexisting phases are equal. In this statistical mechanical framework, the FS transition line $D_c(L, T)$ can be obtained as the locus of points where the two phases are equiprobable, i.e., the areas of the two peaks are equal:⁶⁵

$$\int_0^{\rho_0} d\rho P(\rho) = \int_{\rho_0}^1 d\rho P(\rho) \quad (22)$$

where $\rho_0 \in [\rho_{PM} : \rho_{SG}]$ such that $P(\rho_0) = 0$ (or minimal next to the tricritical point). A way to numerically determine the transition point is, thus, to compare the areas under the peaks of the distributions, cf. Eq. (8).

B. Maxwell “Equal distance” estimate

There are other two methods to determine a first order transition in finite systems, based on the Maxwell construction. If we are in the coexistence region the curve $D(\rho)$ for the system of size L will display a sort of plateau around some $D = D^* \simeq D_c^L$: in a very small interval of D the density changes very rapidly. In the case of a pure state, instead, the $D(\rho)$ curve has a far smoother behavior. In order to estimate the critical point we need to extrapolate the behavior of $D(\rho)$ for the pure phases inside the region of coexistence. To this aim we perform two fits exclusively based on the points outside the spinodal points: for $D < D_{SG}^{sp}$ for the SG phase ($D_{SG}(\rho)$) and $D > D_{PM}^{sp}$ for the PM phase ($D_{PM}(\rho)$). We will call $\rho_{PM,SG}(D)$ the inverse of the curves $D_{PM,SG}(\rho)$ extrapolated from the data points pertaining to the pure PM and SG phases, respectively. The curve $\rho(D)$ will denote the inverse of $D(\rho)$.

In this way we can make a Maxwell-like construction

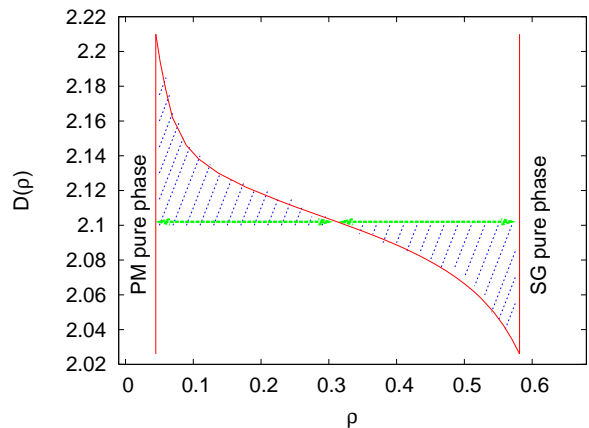


FIG. 1: Graphical sketch of the equal distance (dashed/green arrows) and equal area methods (dotted/blue areas) for FS systems undergoing first order phase transition for a given instance ($L = 6, T = 0.5$).

in the (ρ, D) plane at a given temperature and determine the value of D_c as the one whose corresponding ρ_{ed} value along the $D(\rho)$ FS curve is equally distant from both $\rho_{PM}(D_c)$ and $\rho_{SG}(D_c)$, cf. Fig. 1:

$$\rho_{ed}(D_c) = \frac{1}{2} [\rho_{PM}(D_c) + \rho_{SG}(D_c)] \quad (23)$$

C. Maxwell “Equal area” estimate

Alternatively we can determine D_c as the value at which, cf. Fig. 1

$$\int_{D_{SG}}^{D_c} \rho_{PM}(D) dD + \int_{D_c}^{D_{PM}} \rho_{SG}(D) dD = \int_{D_{SG}}^{D_{PM}} \rho(D) dD \quad (24)$$

where D_{SG} and D_{PM} are arbitrary, provided that they pertain to the relative pure phases.

D. Symmetric distribution estimate

Defining the skewness of the density probability distribution as

$$\zeta(\langle \rho \rangle) = \frac{\langle (\rho - \langle \rho \rangle)^3 \rangle}{\langle (\rho - \langle \rho \rangle)^2 \rangle^{3/2}} \quad (25)$$

in Ref. [66] the critical point was estimated as the point at which the double peaked distribution is symmetric. Since the skewness of $P(\rho)$ can be precisely computed this estimate does not suffer, e.g., of the arbitrariness of the choice of ρ_0 . In the thermodynamic limit, indeed, in the phase coexistence region both peaks of $P(\rho)$ should be Dirac delta distributions and equal weight would be equivalent to a symmetric bimodal distribution. We will show the outcome of this analysis in our system for different cases and compare it with the previous ones.

V. EXCHANGE MONTE CARLO ALGORITHM IN T AND D

We have simulated our spin-1 model using the parallel tempering (PT) algorithm, replicating several copies of the system both at different temperatures and at different values of the external field D . For the PT in temperature, the swap probability of two copies at temperature T and $T + \Delta T$ is:

$$P_{\text{swap}}(\Delta\beta) = \min[1, \exp\{\Delta\beta\Delta\mathcal{H}\}], \quad (26)$$

with $\Delta\beta = 1/(T + \Delta T) - 1/T$; whereas the swap probability in the chemical potential reads

$$P_{\text{swap}}(\Delta D) = \min[1, \exp\{\beta\Delta D\Delta\rho\}] \quad (27)$$

We used the latter implementation in trying to identify the reentrance of the transition line in the T, D plane. Since, however, the transition turns out to be first order in the whole region of inverse freezing, the PT algorithm must be handled with caution. Indeed, at the transition $\Delta\rho$ is discontinuous implying the vanishing of $P_{\text{swap}}(\Delta D)$ around the critical point for a given fix probe ΔD . In order to overcome this problem we have used a varying ΔD , smaller in the candidate coexistence region and larger and larger outside. An instance of this kind choice is represented in Fig. 2.

For very large sizes, though, this would require a too precise *a-priori* knowledge of the transition lines and the method could not be applied with a reasonable success. On the other hand, the FSS effects appear to be almost nonexistent at the first order phase transition, so that probes at larger sizes were actually not necessary. In Tabs. I, II we report our simulation parameters for PT

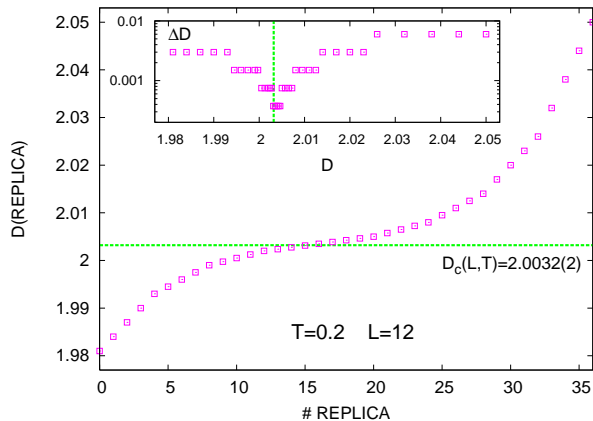


FIG. 2: Values of the chemical potential D for the replicas in the PT simulation exchanging systems at different D . The parameters refer to the simulated $L = 12$ system at $T = 0.2$. The dashed (green) line is the estimate of the FS critical value $D_c(L, T)$ estimated by means of the equal weight method (cf. Sec. IV). Inset: Chemical potential intervals ΔD vs. D in log scale for the same instance.

in temperature and in crystal field, respectively. Thermalization has been checked in three ways.

1. We have verified the symmetry with respect to zero of the site overlap distribution function $P_J(q_s)$ for single random samples (cf, Fig. 3). In absence of an external magnetic field this must be symmetric for any choice of $\{J_{ij}\}$ realization.
2. We have looked at the t -log behavior of the energy and we have considered as thermalized those systems in which at least the last two points coincide within the error, cf. Fig. 3. This means that at least the last half of the data in MCS can be used

$D \downarrow L \rightarrow$		6	8	10	12	16	20	24
0.0	T_{in}	0.6	0.6	0.7	0.7	0.85	0.9	1.0
	N_T	37	37	33	33	27	25	21
	MCS	2^{15}	2^{15}	2^{16}	2^{17}	2^{18}	2^{19}	2^{19}
1.0	T_{in}	0.6	0.6	0.7	0.7	0.7	0.8	0.8
	N_T	37	37	33	33	33	29	24
	- MCS	2^{15}	2^{15}	2^{16}	2^{17}	2^{18}	2^{19}	2^{20}
1.75	T_{in}	0.6	0.6	0.6	0.6	0.6	0.6	0.65
	N_T	37	37	33	33	33	20	22
	- MCS	2^{15}	2^{15}	2^{16}	2^{17}	2^{18}	2^{20}	2^{20}
2.0	T_{in}	0.01	0.01	0.025	0.025	0.3	0.4	0.5
	N_T	90	90	36	36	25	21	17
	- MCS	2^{18}	2^{18}	2^{19}	2^{19}	2^{18}	2^{20}	2^{20}

TABLE I: Simulation parameters of the parallel tempering in temperature: number of samples 2000, Monte Carlo Steps (MCS), number of thermal bath N_T spaced by $\Delta T = 0.02$ or 0.025.

$T \downarrow L \rightarrow$		6	8	10	12	15
0.2	D_{in}	1.99	1.999	2.00392	1.981	1.981
	ΔD_{in}	0.002	0.0006	0.00027	0.003	0.003
	N_D	21	21	37	37	37
	MCS	2^{15}	2^{17}	2^{18}	2^{20}	2^{20}
0.3	D_{in}	2.0034	2.026	2.0212	2.0256	2.028
	ΔD_{in}	0.002	0.001	0.00037	0.003	0.00025
	N_D	21	21	21	31	31
	MCS	2^{15}	2^{17}	2^{17}	2^{17}	2^{18}
0.4	D_{in}	2.05	2.06	2.057	2.06	2.062
	ΔD_{in}	0.003	0.002	0.0007	0.00085	0.0006
	N_D	21	21	21	31	31
	MCS	2^{15}	2^{17}	2^{17}	2^{17}	2^{18}
0.5	D_{in}	2.06	2.06	2.06	2.026	2.026
	ΔD_{in}	0.01	0.01	0.01	0.008	0.008
	N_D	21	21	21	37	37
	MCS	2^{15}	2^{17}	2^{17}	2^{18}	2^{18}

TABLE II: Simulation parameters of the parallel tempering in D . Number of disordered samples: 1000

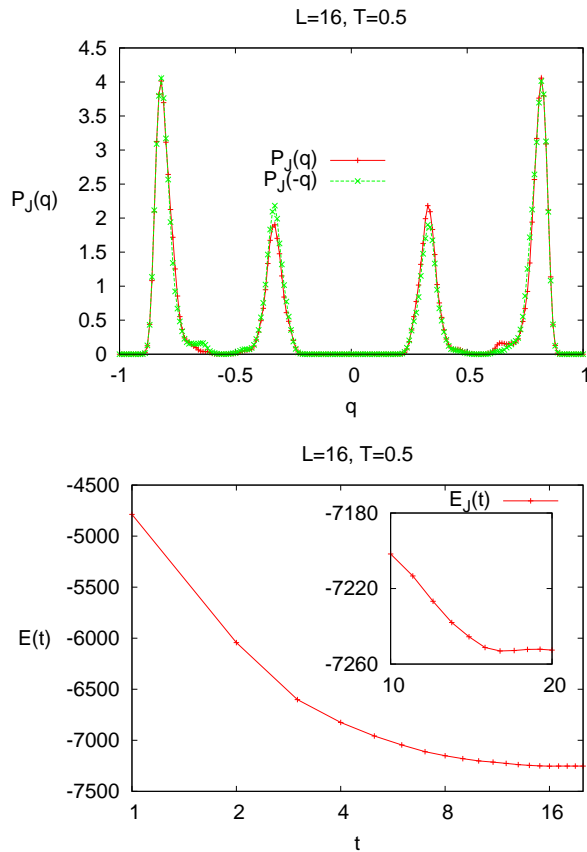


FIG. 3: Instances of thermalization checks. Top: $P_J(q_s)$ and $P_J(-q_s)$ for an arbitrary sample at $D = 0$, $T = 0.5$, $L = 16$. Bottom: average energy versus time (in MCS) in log scale, $t = \log(\#MCS)/\log 2$.

for computing statistical ensemble averages.

- we have checked the lack of variation on logarithmic time-windows of all considered observables (e.g., ξ_c and χ_{SG}) on at least two log points.

VI. NUMERICAL RESULTS.

A. Second order phase transition and universality

In Fig. 4 we present the T -behavior of ξ_c/L for different values of $D = 0, 1, 1.75, 2$ and 2.11 . In the first four cases the curves at different L clearly cross, yielding evidence for a non zero T_c^L . From a FSS $T_c^L = T_c^\infty + aL^{-b}$ we can, thus, extrapolate the critical temperature in the thermodynamic limit. The T_c^L crossing points between $L - 2L$ curves are reported on column 3 of Tab. III. The FSS estimates are reported in columns 2 and 5 of Tab. IV, where L/L' couples are chosen both as $L/2L$ (col. 2) and as contiguous in the series $L = 6, 8, 10, 12, 16, 20, 24$

(col. 5). Analogous, though less precise estimates, can be obtained by studying the behavior of the Binder cumulant g , cf. Eq. (17). Applying both the quotient and the conventional FSS methods we can, eventually, obtain two estimates for the critical exponents.

Before applying these methods, though, we must check if we can exclude cross-over effects as the chemical potential D is varied due to FS. Since we are in presence of a tricritical point, signaled, among others, by the weird behavior of ξ_c/L at $D = 2.11$, cf. Fig. 4, we should control how it influences the results as it is approached along the continuous transition line increasing D . In the mean-field approximation, indeed, at the tricritical point the coefficient of the fourth order term in the SG free energy action goes to zero and the sixth order term becomes relevant for the critical behavior, as shown in Ref. [47]. This is a typical behavior of Blume-Emery-Griffiths-Capel-like systems^{67,68} that might hinder the determination of the critical behavior in the neighborhood of the tricritical point for sizes that are “not large enough”.

D	$L - L'$	$T_c(s)$	$Q_{\partial_\beta \xi}(s)$	$\nu(s)$	$Q_\chi(s)$	$\eta(s)$
0.0	6 - 12	1.02(4)	1.35(1)	2.31(1)	5.1(1)	-0.34(4)
	8 - 16	0.99(6)	1.31(2)	2.58(5)	5.1(1)	-0.36(3)
	10 - 20	1.0(1)	1.35(4)	2.3(1)	5.2(1)	-0.39(4)
	12 - 24	0.98(9)	1.33(2)	2.43(7)	5.1(1)	-0.35(4)
	∞	1.01(1)		2.34(3)		-0.36(1)
D	$L - L'$	$T_c(s)$	$Q_{\partial_\beta \xi}(s)$	$\nu(s)$	$Q_\chi(s)$	$\eta(s)$
1.0	6 - 12	0.894(9)	1.32(1)	2.51(4)	4.9(3)	-0.29(9)
	8 - 16	0.895(9)	1.396(6)	2.08(1)	4.8(4)	-0.26(1)
	10 - 20	0.877(9)	1.271(7)	2.89(2)	5.1(5)	-0.33(1)
	12 - 24	0.86(1)	1.35(1)	2.29(2)	5.1(5)	-0.3(1)
	∞	0.88(1)		2.45(1)		-0.31(2)
D	$L - L'$	$T_c(s)$	$Q_{\partial_\beta \xi}(s)$	$\nu(s)$	$Q_\chi(s)$	$\eta(s)$
1.75	6 - 12	0.715(7)	1.41(1)	*	4.7(5)	*
	8 - 16	0.679(9)	1.37(1)	2.12(4)	4.8(5)	-0.3(1)
	10 - 20	0.67(1)	1.34(3)	2.4(1)	5.0(6)	-0.3(1)
	12 - 24	0.68(1)	1.38(1)	2.11(3)	4.9(5)	-0.3(1)
	∞	0.69(1)		2.20(3)		-0.30(1)
D	$L - L'$	$T_c(s)$	$Q_{\partial_\beta \xi}(s)$	$\nu(s)$	$Q_\chi(s)$	$\eta(s)$
2.0	6 - 12	0.593(7)	1.59(4)	*	9.5(9)	*
	8 - 16	0.569(8)	1.47(3)	*	18(2)	*
	10 - 20	0.54(1)	1.37(3)	*	16(2)	*
	12 - 24	0.54(1)	1.34(4)	*	10(2)	*
	∞	0.56(1)				

TABLE III: Critical temperature and exponents are calculated with QM: for $D = 0.00$, $D = 1.00$ and $D = 1.75$, through a FSS analysis of the values of $Q_{\partial_\beta \xi}(s)$ and $Q_\chi(s)$ for $s = L'/L = 2$. Cells with * mean that quotients are computed on sizes too small to significantly represent the asymptotic behavior with L .

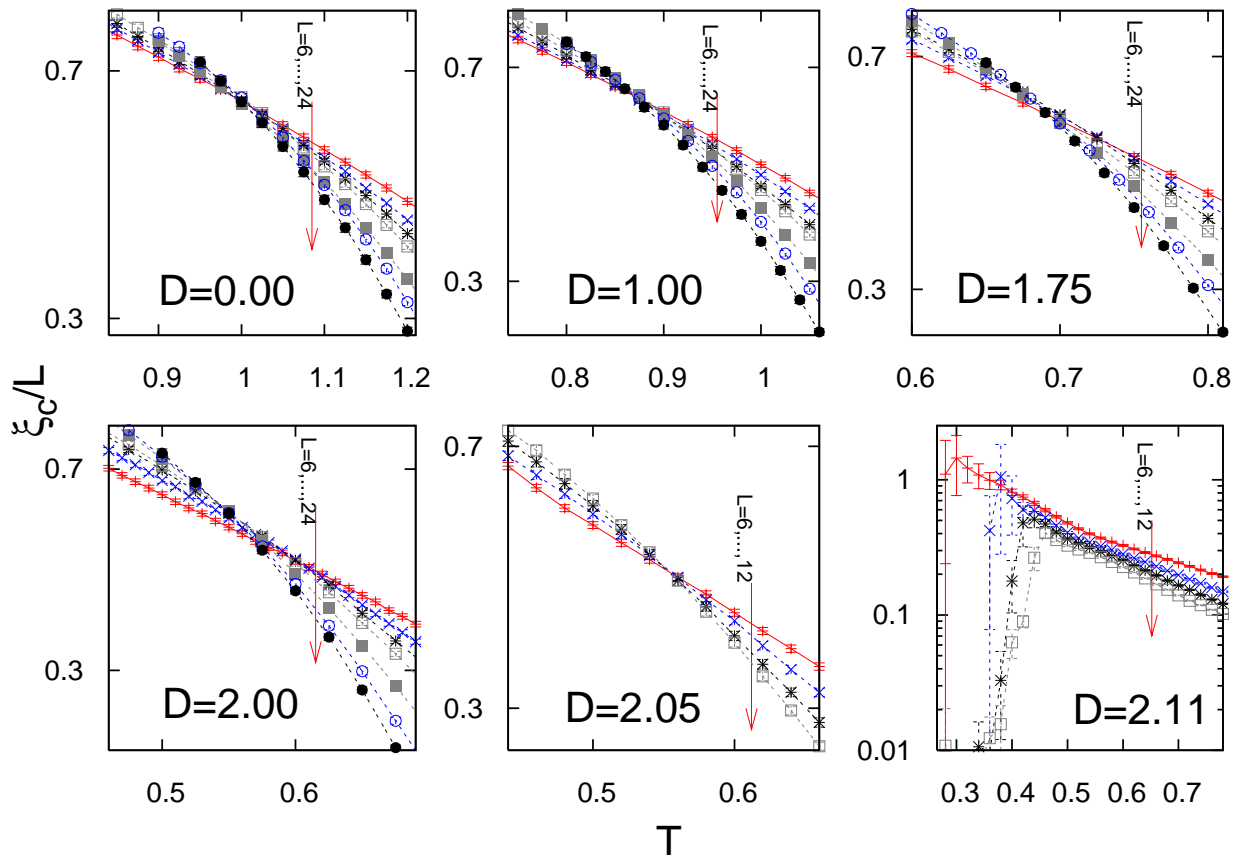


FIG. 4: Scaling functions ξ_c/L vs. T for different values D . For $D = 0, 1, 1.75, 2$ ($L = 6, 8, 10, 12, 16, 20, 24$) evidence for a continuous phase transition is found in the region of scale invariance. At $D = 2.11$ ($L = 6, 8, 10, 12$) no crossing is observed and, at low T , $\xi_c/L \rightarrow 0$.

To estimate and control FS effects we use the scaling methods introduced in Sec. III and compare different universal FSS functions. In Fig. 5 we plot the Binder parameter g vs. the rescaled correlation length ξ_c/L at all simulated values of the chemical potential D both for a small ($L = 6$, top) and a large ($L = 20$, bottom) system. In the top plot one can easily observe that as the tricritical value of D is approached ($2.05 < D_{3c} < 2.11$) for $L = 6$ the curves do not overlap with each other signaling an apparent lack of universality. At large enough sizes, instead, all curves are superimposed (bottom plot of Fig. 5, $L = 20$), demonstrating that universality holds along the whole continuous transition line and that, because of strong FS effects, a crossover occurs and the analysis limited to (or including also) too small sizes can hinder the prediction of the asymptotic behavior.

The same effect is clearly shown in Fig. 6 where the size dependence of spin-glass susceptibility at criticality is shown. As D increases towards D_{3c} there appears to be a crossover in the scaling moving from small to large sizes and induces wrong asymptotic values of the critical indices. We, thus, did not make use of the small values of L for $D \simeq D_{3c}$, namely $L = 6$ at $D = 1.75$ and $D = 6, 8, 10$ and 12 at $D = 2$, to interpolate the values of

the critical exponents, as they induce a wrong estimate as the limit $L \rightarrow \infty$ is performed.

As a test for the eye, in Fig. 7, we display g vs. ξ_c/L for all D and L values employed for our FSS analysis. Without the smallest sizes near the tricritical point, universality appears quite tidy. In Fig. 8 we parametrically plot the universal FSS functions F_ξ , $F_{\chi_{SG}}$ and F_g , cf. Sec. III, vs. ξ_c/L , as well, for the same simulated systems.

The critical values of the temperature and the expo-

D	T_c	ν	η	T_c	ν	η
0.00	1.01(1)	2.34(3)	-0.36(1)	1.0(1)	2.5(2)	-0.37(2)
1.00	0.88(1)	2.45(1)	-0.31(2)	0.8(1)	2.6(5)	-0.31(2)
1.75	0.68(2)	2.20(3)*	-0.30(1)*	0.6(1)	2.6(6)	-0.30(4)
2.00	0.56(1)	†	†	0.5(1)	2.3(2)	-0.31(2)

TABLE IV: Critical temperature and exponents calculated via QM $Q_{\partial\beta\xi}(s, T_c(s))$ and $Q_{\chi_{SG}}(s, T_c(s))$ (cols. 2,3 and 4) and via standard FSS analysis of the behavior of $\log \partial\xi_c(L, T_c(L))/\partial\beta$ and $\log \chi_{SG}(L, T_c(L))$ (cols. 5, 6 and 7). *: estimated through QM without $L = 6$. †: not estimated by QM.

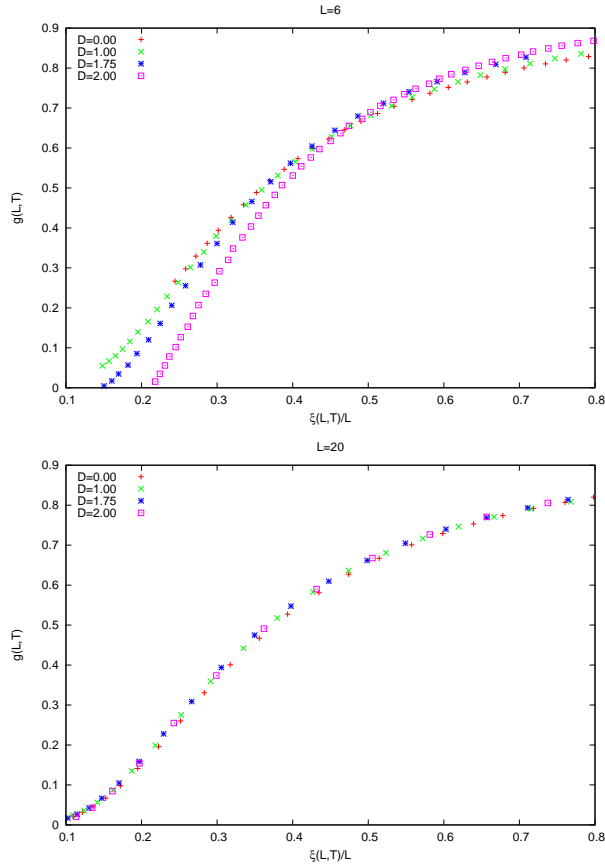


FIG. 5: Universal scaling function g vs. ξ_c/L at $L = 6$ (left) and $L = 20$ (right) for all simulated D values. At small size the curves do not fall on top of each other as D is too near the tricritical point $D = 1.75, 2$, whereas at large size their critical behavior appears to be the universal for all D .

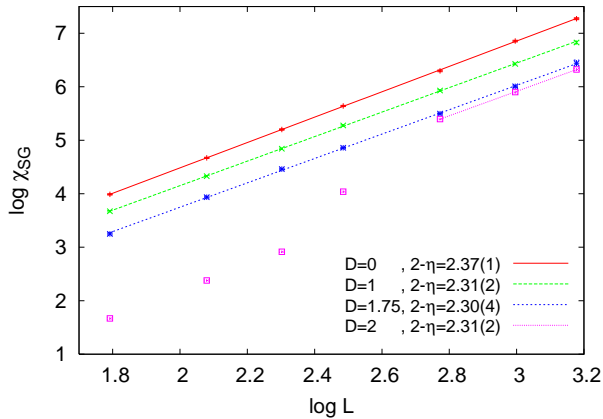


FIG. 6: χ_{SG} vs. L in log-log plot for $D = 0, 1, 1.75, 2$. For $D = 2.00$, near the tricritical point, a cross-over is evident from small ($L \lesssim 12$) to large ($L > 12$) sizes. The quotient method does not yield reliable estimates because of a crossover in the scaling functions in the range of probed sizes.

nents η and ν are shown in Tab. IV both for the QM and

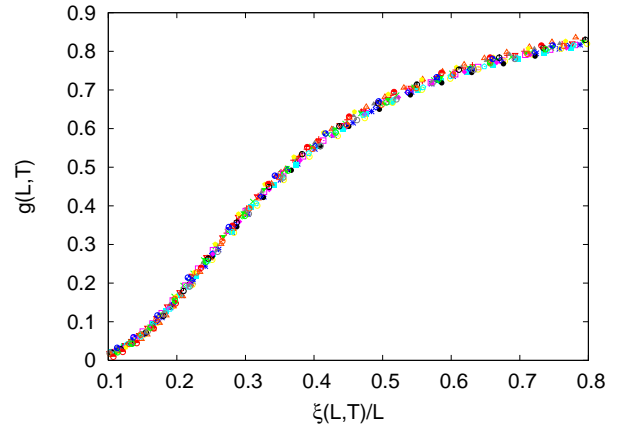


FIG. 7: Binder parameter $g(L, T_c(L))$ vs. $\xi_c(L, T_c(L))/L$ in the critical region for different D and L . Values of $L = 6, 8, 10, 12$ for $D = 2$ and $L = 6$ for $D = 1.75$ are omitted.

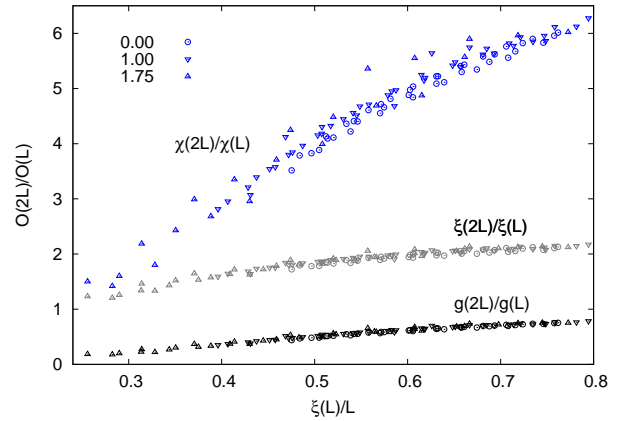


FIG. 8: Scaling behavior of $F_{\chi_{SG}}, F_{\xi}$ and F_g (top to bottom) vs. $\xi_c(L, T)/L$, cf., respectively, Eqs. (14), (13), (17) and (18), at $D = 0, 1, L/2L = 6/12, 8/16, 10/20, 12/24$ and at $D = 1.75, L/2L = 8/16, 10/20, 12/24$.

Model	ν	η
SG 3D bd ⁶⁹	2.22(15)	-0.349(18)
SG 3D bd ⁷⁰	2.53(8)	-0.384(9)
EA 3D ⁷¹	2.15(15)	-0.337(15)
EA 3D ⁷²	2.00(15)	-0.36(6)

TABLE V: Critical Indices of EA models in literature

the canonical FSS methods. Due to the FS cross-over no interpolation was possible with QM at $D = 2$. We, thus, provide only one estimate for the indices.

As one can see, comparing with estimates of critical exponents summarized in Tab. V, the system appears to be in the same universality class of the Edwards-Anderson model (corresponding to the $D = -\infty$ limit of our model).^{71,73-75}

In Fig. 4 we also plot ξ/L at $D = 2.05$ and $D = 2.11$

for $L = 6, 8, 10, 12$. In the first case we obtain a $T_c = 0.553(7)$, though no analysis of the critical exponents can be performed because of FS effects. In the latter case no evidence is found for a second order phase transition, cf. Fig. 4. As $T \lesssim 0.5$ is approached, moreover, ξ even appears to scale weaker than L . We will see in the following why this comes about.

B. First order phase transition

Across a second order transition the system undergoes a transformation from a PM pure phase to a SG pure phase. As far as the density distribution $P(\rho)$ is concerned, a pure phase corresponds to a single-peaked distribution. As two peaks appear, the system exists both in PM (low ρ) and SG (high ρ) coexisting phases and we are in the neighborhood of a first order phase transition. In FS systems the peaks are not delta-shaped but become sharper and sharper as L increases. At finite L , thus, $P(\rho)$ is a good order parameter that drives the first order kind of transition: varying D, T , the system undergoes a transition with a discontinuous jump in ρ and the “thermodynamic” average values of ρ are obtained by looking at the peaks of its distribution.

In Fig. 9 we show the behavior of the density distribution through the first order transition at $T = 0.4$. The FS first order transition points can be determined with the four methods mentioned in Sec. IV, as we will show below. The spinodal lines at given L are estimated by looking at the D values at which a secondary peak arises. Since the region of phase coexistence corresponds to an inverse freezing transition, we performed PT simulations at finite T , changing D . Indeed, in our model, we will see that the first order transition line displays a reentrance^{40,49} due to the existence of a “fluid” (PM) phase with an entropy lower than the one of the glassy phase.

For what concerns the estimate of $D_c(T)$ the method of *equal weight* introduced in Sec. IV, cf. Eq. (22) works quite well for data collected at $T \leq 0.4$, because the two peaks are very well separated as soon as they appear, cf. Fig. 9, and the estimate is robust against reasonable changes of ρ_0 (see inset of Fig. 9). As T increases towards the tricritical value, however, the PM and SG values of the density approach each other. At $T = 0.5$, cf. Fig. 10, we thus have the problem that the distributions of the densities of the two phases are overlapping also for the largest simulated size. In that case, seen the arbitrariness of choosing ρ_0 , we actually determine the transition point as the D value at which the peaks have the same height. This is a rough estimate but yields no difference w.r.t., e.g., fitting the two peaks separately and computing the areas under the interpolating curves. In Tab. VI we report for all simulated sizes and temperatures the estimated values of the critical points obtained by this method, together with the spinodal points.

These results can be cross-checked using the methods

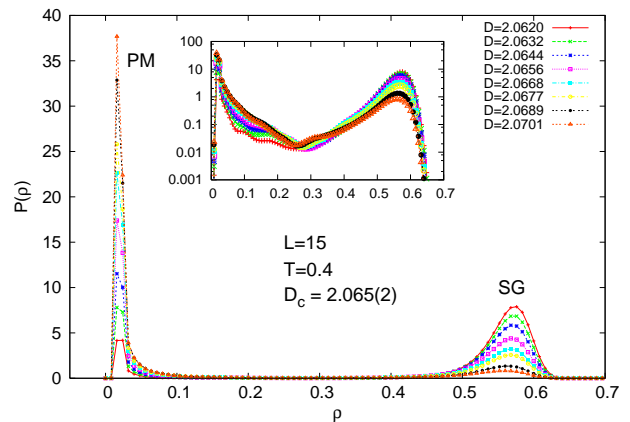


FIG. 9: Density distribution $P(\rho)$, $L = 15$, across the coexistence region at $T = 0.4$: two peaks develop at ρ_{PM} and ρ_{SG} . As D increases the thermodynamically relevant phase (lowest free energy) passes from SG to PM in a first order phase transition. The dominant phase corresponds to the one with larger probability, i.e., larger integral of the peak. As the peak at ρ_{SG} vanishes the system is in a purely PM phase. Inset: $P_{15}(\rho)$ on y -Log scale.

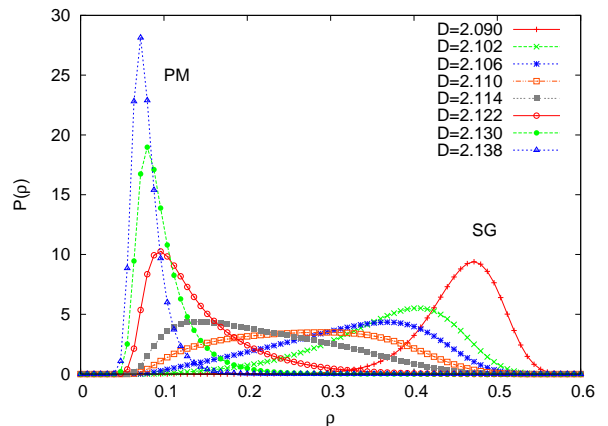


FIG. 10: $P(\rho)$ in the coexistence region at $T = 0.5$ and $L = 15$. The two peaks are hard to distinguish and the coexistence region is rather narrow.

based on the Maxwell construction, cf. Sec. IV and Fig. 11. The pure phase behaviors $D_{PM,SG}(\rho)$ are interpolated in the coexistence region by a polynomial fit on those points for which no double peak is present in the $P(\rho)$. At any given L we look at the value $D = D_c$ such that (equal distance)

$$\rho_{SG}D_c - \rho(D_c) = \rho(D_c) - \rho_{PM}(D_c)$$

and at the value of $D = D_c$ at which the areas between D_c and $D(\rho)$ to the left and to the right of their crossing point are equal, i.e.,

$$\Delta\mathcal{A}(D_c) = \int_0^{\rho(D_c)} d\rho'(D(\rho') - D_c) - \int_{\rho(D_c)}^1 d\rho'(D(\rho') - D_c). \quad (28)$$

T	D_c	D_{SP}^{PM}	D_{SP}^{SG}
0.2	2.0031(1)	1.9833(2)	2.024(1)
0.3	2.032(3)	2.015(1)	2.043(5)
0.4	2.060(1)	2.046(2)	2.092(5)
0.5	2.106(1)	2.097(4)	2.143(4)

TABLE VI: Results of the first order phase transition: a fine tuning of the parameters $\{D_i\}$ is needed in order to establish the critical values D_c , D_{SP} and D_{SG} .

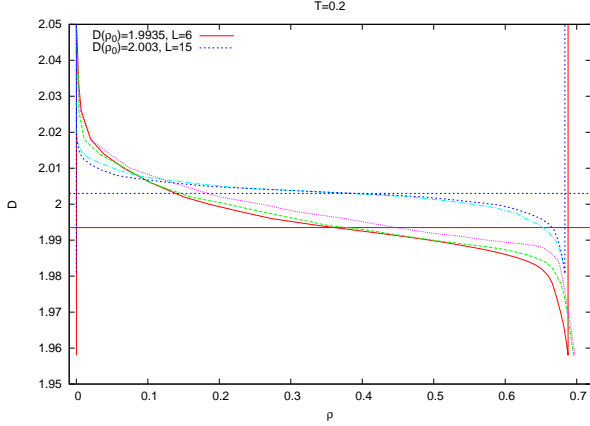


FIG. 11: Maxwell construction at $T = 0.2$ in the ρ , D plane. $L = 6, 8, 10, 12, 15$ from bottom to top as $\rho \gtrsim 0.6$ (right). The almost vertical lines at the small and large density sides are the interpolated pure phase (PM left, SG right) behaviors. As an instance the critical D values for the equal distance construction are plotted at $L = 6$ (lower horizontal line) and at $L = 15$ (higher horizontal line).

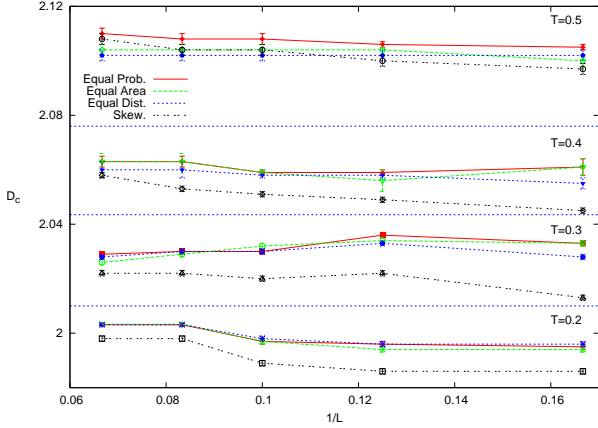


FIG. 12: Estimates of D_c vs. $1/L$ for $L = 6, 8, 10, 12, 15$ at $T = 0.2, 0.3, 0.4, 0.5$ (bottom up) obtained by the four methods described in Sec. IV.

is zero.

We, eventually, compute the skewness of double peaked $P(\rho)$ as D changes, looking at the $D = D_c$ point for which $\zeta(\rho(D_c)) = 0$. Since the two peaks of $P(\rho)$ at finite size appear to be of different shape (SG broader,

T	$D_c[P(\rho)]$	$D_c[\rho_{ed}]$	$D_c[\Delta\mathcal{A} = 0]$	$D_c[\zeta = 0]$
0.2	2.0031(1)	2.0033(2)	2.0031(2)	1.991(2)
0.3	2.032(3)	2.031(2)	2.030(1)	2.020(2)
0.4	2.060(1)	2.060(1)	2.058(1)	x
0.5	2.106(1)	2.103(3)	2.102(1)	x

TABLE VII: Evaluation of the first order critical point with the method of equal weight (col. 2), equal distance (col. 3), equal area (col. 3) and zero skewness.

PM narrower), cf. Figs. 9, 10, the point at which the skewness is zero appears to be slightly different from the D_c values computed with the previous three methods. In Fig. 12 we plot at different temperatures the FS values of $D_c(L)$ with the four methods. The equal weight method and the two Maxwell construction methods yield consistent results. For $T = 0.4, 0.5$ the estimate of D_c by the symmetric distribution method displays a growing behavior in $1/T$ that does not allow for a consistent $L \rightarrow \infty$, cf. Fig. 11 first and second panel from top, whereas at lower temperature, where the interpolated thermodynamic limit is stable the value is smaller than the other estimates.

Summarizing, in Tab. VII we report the estimates of the first order critical point obtained by means of the four methods.

C. Phase diagrams and inverse freezing

Phase diagrams are plotted in Fig. 13. In the D, T plane we observe a pure SG phase at low T and $D \lesssim 2$. Increasing the temperature the continuous transition to the pure PM phase is denoted by a full line connecting the five numerical estimates of T_c obtained by simulations at $D = 0, 1, 1.75, 2$ and $D = 2.05$. We found no evidence for a continuous phase transition at $D = 2.11$. Beyond $(D, T) = (2.05, 0.53(2))$ a tricritical point is placed. Beside changing to a first order transition, for lower T also a reentrance in the $T_c(D)$ line occurs. The warmest first order point for which we have an estimate is $(D, T) = (2.109(2), 0.5)$. In Fig. 14 a detail of the phase coexistence region is plotted (inside the grey-dotted lines). In the inset of Fig. 13 we plot the (ρ, T) diagram. Below $T = 0.53(2)$ no pure phase exists with an average ρ in between the dashed-grey curves.

The inverse freezing takes place between a SG of high density to an almost empty PM (e.g., at $T = 0.4$, in the coexistence region $D \in [2.046(2) : 2.092(5)]$, $\rho_{SG} \simeq 0.52$ and $\rho_{PM} \simeq 0.03$). The few active sites do not interact with each other but only with inactive neighbors and this induces zero magnetization and overlap. The corresponding PM phase at high T has, instead, higher density (e.g., $\rho_{PM}(D = 2, T = 0.6) = 0.4157(2)$, $\rho_{PM}(D = 2.11, T = 0.6) = 0.596(2)$) and the paramagnetic behavior is brought about by the lack of both magnetic order (zero magnetization) and blocked spin

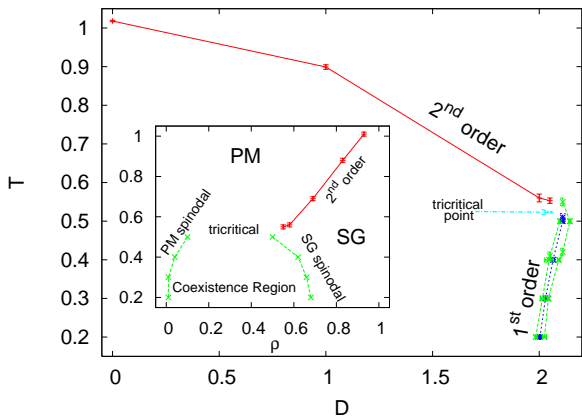


FIG. 13: Phase diagram in D, T : second order transition and an inverted first order phase transition occur. In the latter case also the spinodal lines are reported (dashed). Inset: T, ρ phase diagram.

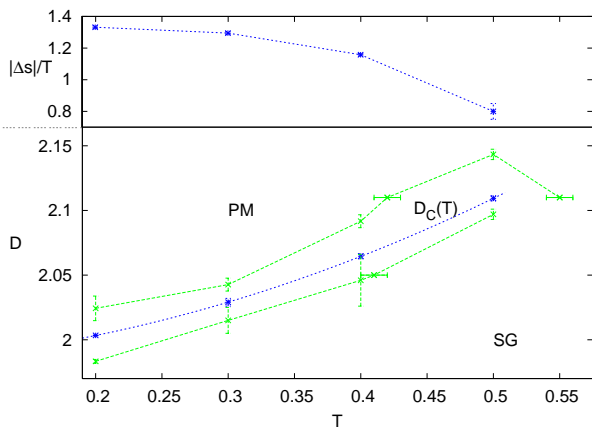


FIG. 14: Detail of inverse freezing region, interpolation of transition line $D_c(\infty, T)$ (dotted), spinodal lines (dashed). The error bars are the FSS of the minimal interval in T and D at each L needed to identify the crossings in ξ_c/L curves (for continuous transitions) or compare the areas under $P_N(\rho)$ for first order transition. In the top inset we show the latent heat $|\Delta s|/T$ along the first order transition line.

configurations (zero overlap).

Using Eq. (21), from the knowledge of $\Delta\rho$ and the numerical estimate of dD/dT we are able to evaluate the latent heat employed in the transition, that we plot as a function of temperature in the top inset of Fig. 14.

VII. NATURE OF THE SG PHASE.

The SG phase of the disordered BEG model, in mean-field regime, shows the same features of the Sherrington-Kirkpatrick model:⁷⁶ in order to obtain a stable thermodynamics the Full RSB scheme is needed.^{47,48} On the other hand, out of the limit of validity of the mean-field

regime, it is still unclear if the properties of SG phase are in agreement with the RSB scenario. The low T, D phase is characterized by a pure spin-glass phase and what this phase consists of in terms of statistical mechanic states is the subject of the following analysis. Three cases are contemplated in the literature.

Droplet theory: it exists only one SG state (plus its symmetric spin-reversed) and, therefore, the overlaps between states in different replicas cannot fluctuate among different disordered samples and the distributions are delta-shaped.⁷⁷ The four-spins correlation function in position space $\mathbf{r} = (x, y, z)$ should tend to a plateau $C_4(|r|) = q_{EA}^2$, for large enough $|r|$, that becomes longer as T decreases towards T_c .

Trivial-Non-Trivial (TNT) scenario: equilibrium states are many and non-trivially organized (i.e., q_s fluctuates from sample to sample), but the excited states are droplet-like (i.e., the q_l overlap, sensitive to interfaces, fluctuates less and less as the size grows). This implies that $P(q_s)$ is broad and non-trivial, whereas $P(q_l)$ is delta-shaped.⁷⁸ Since excitations are trivial, the expected behavior of $C_4(x, y, z)$ is the same as for the droplet theory.

Replica Symmetry Breaking (RSB) theory: many states characterize the SG phase, with space-filling excitations; both distributions are, thus, broad, with a complex structure.^{61,79} The correlation $C_4(x, y, z)$ is expected to decay continuously to zero (the minimum squared overlap for the present system, in absence of an external magnetic field) at all T .^{81,82}

First we will consider the overlap distribution functions, cf. Eqs. (6)-(7), since, in the spin glass phase ($T < T_c$), the site and the link overlap distributions - $P(q_s)$ and $P(q_l)$ - can be used as hallmarks to discriminate among different theories for finite dimensional spin glasses. In the next section we will analyze the four spin correlation functions.

In order to see whether $P(q_s)$ is trivial or not we need to estimate if, for growing sizes its support does shrink to a unique value, the Edwards-Anderson parameter q_{EA} or it remains finite. In our case, in absence of an external magnetic field, the support of a non-trivial $P(q_s)$ should range from $q_s = 0$ to q_{EA} . In Fig. 15 we plot $P(q_s)$ at $D = 0$ and size $L = 16$ for all simulated temperatures: as T decreases $P(q_s)$ moves from a Gaussian to a bimodal distribution. The important issue is, then, whether the continuous part in between the two peaks at low T goes to zero or not as L increases. In Fig. 16, we plot $P(q_s)$ at the lowest thermalized temperature for $L = 6, 8, 10, 12$ and 16 and, in the inset, we plot the values of $P_L(0)$ displaying no decreasing trend with increasing L . The states, thus, appear to be many and different among themselves, since they are found with a finite probability within a non-zero continuous range of overlap values, including $q_s = 0$.

Also $P(q_l)$ appears to develop a second peak at small q_l as L increases, and this signature becomes clearer and clearer at low temperature as L increases, cf. Fig. 17.

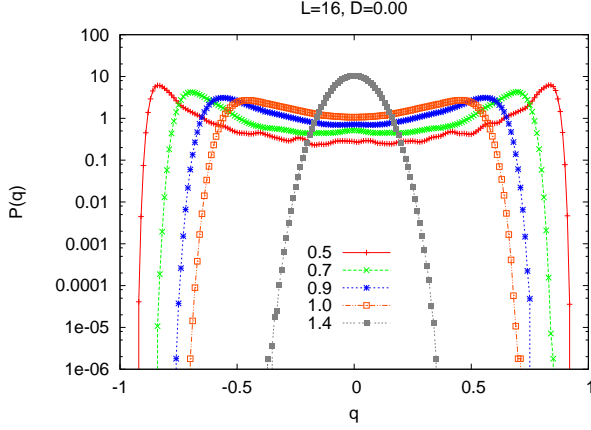


FIG. 15: Behavior of the overlap distribution $P(q)$ through the second order phase transition and in the low-temperature phase for $L = 16$.

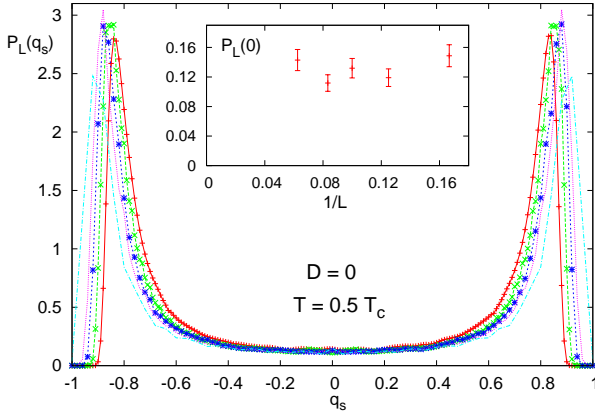


FIG. 16: Site overlap distribution $P_L(q_s)$ at $T = 0.5$, $D = 0$ for $L = 6, 8, 10, 12, 16$. Inset: $P_L(0)$ vs. $1/L$ does not tend to zero.

The analysis of FSS of the variance of $P(q_l)$ might help to better evaluate the breadth of the distribution in the thermodynamic limit. Its behavior for various sizes is exemplified in the inset of Fig. 17 at the lowest T/T_c we simulated for $D = 0$. The variance tends to a small finite value and we cannot make a definitive statement about $P(q_l)$ tending towards a delta distribution, as conjectured by the TNT scenario. Moreover, the study of the variance does not yield any indication about the *shape* of the distribution. In particular, about the FSS behavior of the two peaks expected in RSB theory.

A. Equivalence of site and link overlap distributions

We can, then, implement a more refined analysis of the pdf data and check whether $P(q_s)$ and $P(q_l)$ are actually equivalent and, thus, if the non-triviality of the former

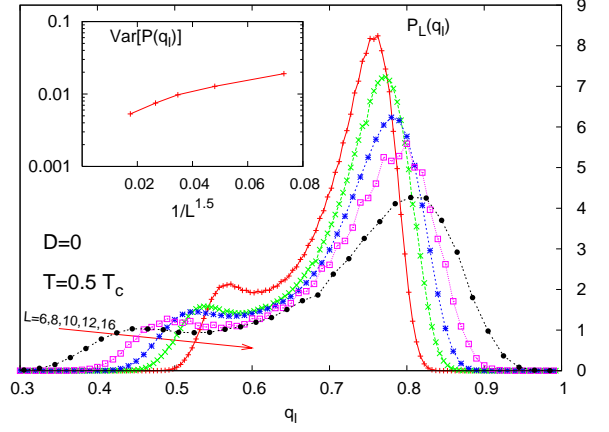


FIG. 17: Link overlap distribution $P_L(q_l)$ at $T = 0.5$, $D = 0$ for $L = 6, 8, 10, 12, 16$. Inset: Variance vs. $1/L$ tends to a very small value $\sigma_{q_l}^2 = 0.0010(7)$ as $L \rightarrow \infty$ interpolating with a power-law (1.5(1)).

implies the non-triviality of the latter. This can be realized by recalling that in the SK model $q_l = q_s^2$ and by comparing $P(q_l)$ to the distribution $Q(q_a)$ of an auxiliary variable

$$q_a \equiv A + Bq_s^2 + z\sqrt{1 - q_s^2} \quad (29)$$

with z a Gaussian random variable of variance σ_z and zero mean, that mimics the presence of fluctuations due to the finite size of the considered systems.

At a given point of the phase diagram D, T and for a given size L , the parameters $A(L)$, $B(L)$ and $\sigma_z(L)$ can be obtained by minimizing the Kullback-Leibler divergence⁸⁰ (KLD) between $P(q_l)$ and $Q(q_a)$:

$$D_{\text{KL}}[P, Q] = \sum_{i=1}^{N_{\text{bin}}} P(q_i) \log \frac{P(q_i)}{Q(q_i)} \quad (30)$$

We will refer to this one as the “left” KLD. The “right” KLD is the same formula exchanging P and Q , where the symmetrized divergence (sKLD) between $P(q_l)$ and $Q(q_a)$ is defined as:⁸²

$$D_{\text{KL}}[P, Q] = \frac{1}{2} \sum_{i=1}^{N_{\text{bin}}} \left[P(q_i) \log \frac{P(q_i)}{Q(q_i)} + Q(q_i) \log \frac{Q(q_i)}{P(q_i)} \right] \quad (31)$$

In Fig. 18 we plot, the finite size values of the parameters A and B . Besides the values of the parameters minimizing the symmetrized KLD, Eq. (31) we also plot the values of A and B minimizing the left and the right unsymmetrized KLD’s. We observe that, as L increases the spread between different estimates tends to vanish. The infinite size limit of σ_z is always compatible with zero, signaling that FS effects actually tend to vanish as L increases, though with large statistical errors at low temperature, implying that smaller sizes might hinder a correct FSS.

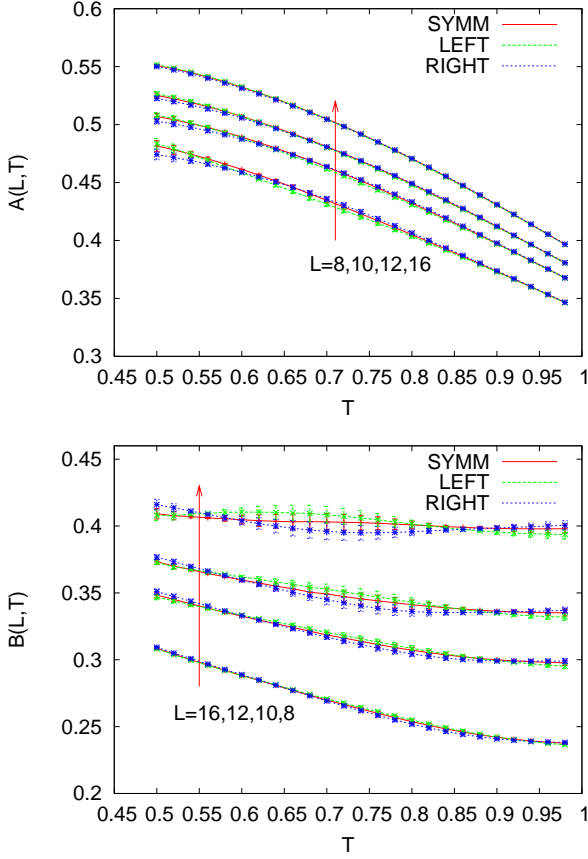


FIG. 18: Parameter A (top) and B (bottom) of q_a vs. T for $L = 8, 10, 12, 16$ as obtained minimizing the left, right and symmetric Kullback-Leibler divergence.

As instances we plot the matching of the two distributions $Q(q_a)$ and $P(q_l)$ in Figs. 19 at $T = 0.5 \simeq 0.5T_c$ and $T = 0.7 \simeq 0.7T_c$ at size $L = 16$ and $D = 0$. In the insets we plot the size behavior of A and B from the sKLD for the two specific cases. In the first case, performing a power-law FSS scaling to $L \rightarrow \infty$ we obtain that B interpolates a negative value! In the second case the $L \rightarrow \infty$ limit yields a positive value. This observation is contrasting from the behavior, cf. bottom panel of Fig. 18, of $B(T)$ growing with decreasing T at all fixed sizes. Quite evidently, the low L strong fluctuations strongly bias the interpolation at small T . To show it in a clearer way, in Fig. 20 we plot the asymptotic values of both A and B for all simulated temperatures both from the sKLD and as the average of the extrapolation of the values minimizing the right and left unsymmetrized KLD's. With $A_\infty(T)$ the two estimates appear to be consistent at all temperature and reproduce the qualitative behavior detected in all finite L cases, compare with Fig. 18. For $B_\infty(T)$, at low T the two estimates are not consistent anymore. Moreover, $B_\infty(T)$ decreases with T below a certain $T \simeq 0.7$, unlike its finite L counterparts (at least as $L \geq 10$), cf. Fig. 18.

We face strong finite size effects and a crossover be-

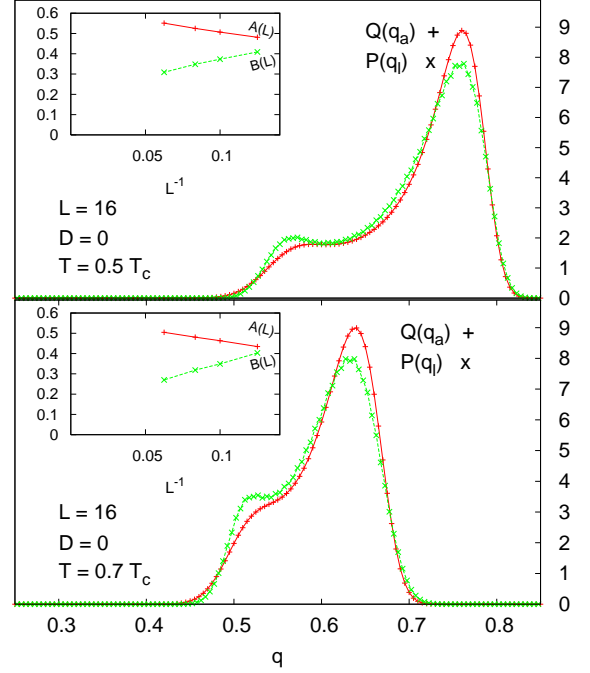


FIG. 19: The distributions $Q(q_a)$ and $P(q_l)$ at $T = 0.5 \simeq 0.5T_c$ (top) and $T = 0.7 \simeq 0.7T_c$ (bottom), $D = 0$ for an optimal choice of parameters obtained by minimizing sKLD, cf. Eq. (31). Inset: FSS behavior of the parameters $A(L)$ and $B(L)$ of the sKLD between $Q(q_a)$ and $P(q_l)$ at $D = 0$ and $T = 0.5 \simeq 0.5T_c$. Sizes are for $L = 6, 8, 10, 12, 16$.

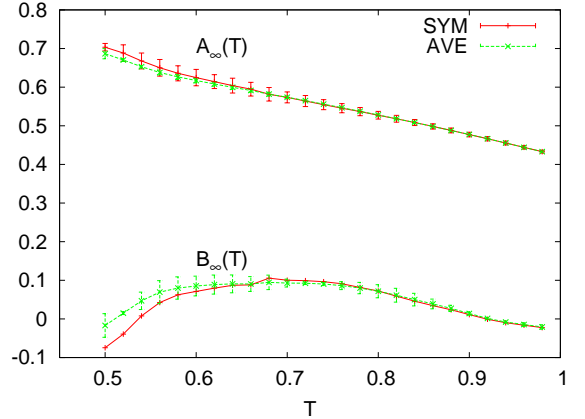


FIG. 20: FSS limit $L \rightarrow \infty$ of A and B parameters vs. T .

tween small and large sizes is taking place. However, due to the fact that we cannot easily thermalize larger systems at low temperature, we cannot make any definite statement on the behavior of $B_\infty(T)$ for very low T . We simply do not have enough reliable points in L at our disposal. The finite size behaviors, though, strongly suggest that $Q(q_a)$ and $P(q_l)$ are, indeed, equivalent even below $T = 0.7$. In any case, the equivalence is proven for $T \geq 0.7$ implying that not only the equilibrium states have a non-trivial distribution but also their excitations,

yielding evidence in favor of the third scenario considered, the RSB theory, rigorously valid in mean-field systems.

B. Position Space Four Spins Correlations

We now investigate the behavior of the four spins correlation function, defined in Eq. (10), in position space. We recall that the droplet and TNT theories predict that $C_4(x)$ tends to a plateau of height q_{EA}^2 (cf. Sec. VII) whereas RSB theory predicts for $C_4(x)$ at $T < T_c$ a power-law decay $\sim x^{-\alpha}$. We, thus, have to compare our data with the prediction of one of these hypotheses.

Since we are dealing with small systems, we must first consider possible FS effects. Indeed, because of the periodic boundary conditions imposed on the simulated system, the correlation function that we actually measure at a distance x also contains the contribution of correlations at distance $x + kL$, with $k = 1, \dots, \infty$ and the true (yet unknown) correlation function $C_4(x, y, z)$ is related to the measured one - $C_4(x, y, z)$ - by the relationship:

$$C_4(x, y, z) = \sum_{k_x, k_y, k_z}^{0, \infty} C_4(x + k_x L, y + k_y L, z + k_z L) \quad (32)$$

For large distances, when C_4 is smaller, these extra contribution will strongly bias the estimate of the true C_4 behavior in space. In particular, correlations at larger distances, of order $L/2$, will experience relatively stronger systematic errors than $C_4(|r| \ll L)$.

We will now present our results for the case $D = 0$. For temperatures down to the critical region we simulated lattices with sides of length up to $L = 24$. The largest thermalized size for T down to $0.5T_c$ is, instead, $L = 16$. In Fig. 21 we plot the x behavior at $T = 1.5$ in a log-log plot for the sizes 10, 12, 16, 20, 24. One can observe that FS effects are limited to the last point at $L/2$. The rest of the curves completely superimpose.

At high temperature, correlations are expected to decay exponentially at large enough distances. As temperature is lowered towards criticality the $C_4(x)$ should become power-law eventually decaying as $x^{-d+2-\eta}$ at $T = T_c$. We, then, interpolate the four-spins correlation function along the x -axis at criticality with the function:

$$C_4^{\text{fit}}(x) = ax^{-\alpha} \left[1 + \left(\frac{x}{\ell} \right)^{-\delta\alpha} e^{\delta x/\ell} \right]^{-1/\delta} \quad (33)$$

and equivalently for y and z , due to the anisotropy of the system in absence of an external field. This is a function containing a crossover between a short distance power-law decay, $x^{-\alpha}$, and an exponential decay, with characteristic 'correlation' length ℓ . In Fig. 21 the function interpolating the $L = 24$ $C_4(x, 0, 0)$ is plotted with $a = 0.402(9)$, $\delta = 0.69(1)$, $\ell = 1.25(1)$ with $\chi^2 = 0.088$. As the temperature decreases the correlation length increases until it becomes too long to be observed in the

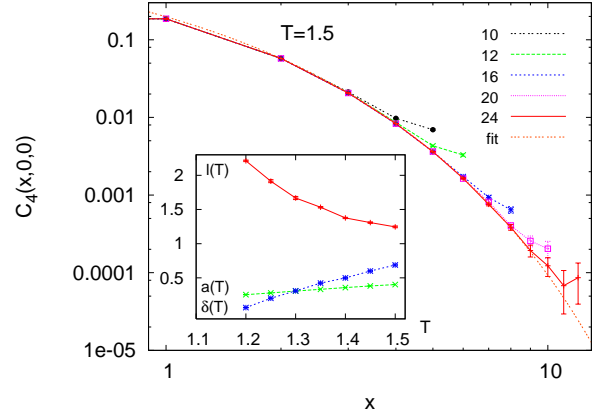


FIG. 21: Correlation between local overlap for $D = 0$ and sizes $L = 10, 12, 16, 20, 24$, at the largest simulated temperature $T = 1.5$. The fit with Eq. (33) is also plotted.

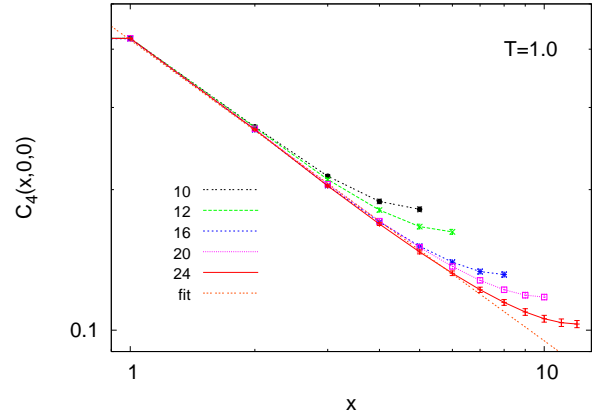


FIG. 22: Behavior of $C_4(x)$ at $D = 0$, for $L = 10, 12, 16, 20, 24$ and $T = 1 \simeq T_c$. The interpolation with a simple power-law, $\alpha = 0.64(1)$, is shown for $L = 24$. On shorter systems: $\alpha = 0.64(1)$, $L = 20$ and $\alpha = 0.65(2)$, $L = 16$.

analyzed systems. In the inset of Fig. 21 we plot the T behavior of ℓ , α and δ until the fit becomes inconsistent $T \simeq 1.15$.

In Fig. 22 we plot the C_4 curves at $T \simeq T_c$ for sizes $L = 10, 12, 16, 20, 24$, as well as the interpolation of the latter with $Ax^{-\alpha}$ (the correlation length is too long to detect the exponential contribution in Eq. (33)). The exponent equals the power at criticality $\alpha = d - 2 + \eta = 0.64(1)$ (at crystal field $D = 0$ it was $\eta = 0.36(1)$, cf. Tab. III). At $T = 1$ the interpolated value of α for the $L = 24$ $C_4(x)$ curve is $\alpha = 0.64(1)$, $\alpha = 0.65(2)$ for $L = 16$ and $\alpha = 0.64(1)$ for $L = 20$. FS effects appear to be stronger now w.r.t. Fig. 21 and evident also for $x < L/2$ (only points for $x \leq L/4$ actually stay on the $x^{-\alpha}$ curve).

Approaching T_c , as $T < 1.2$, cf. Fig. 23, it is not possible to detect a crossover between power-law and exponential decay and the simple power-law decay is tested. In the inset the power behavior in T is shown and com-

VIII. CONCLUSIONS

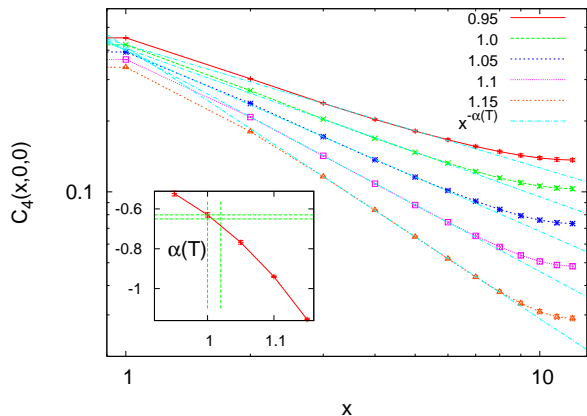


FIG. 23: Behavior of $C_4(x)$ for $L = 24$ and $T = 0.95, 1, 1.05, 1.1, 1.15$. The interpolation with a simple power-law is also shown for $L = 24$. Inset: behavior of the power α vs. T . The dashed vertical and horizontal lines denote, respectively the estimates of $-d + 2 - \eta$ and T_c (with errors, cf. Tab. IV: $T_c = 1.01(1)$, $\eta = -0.35(1)$).

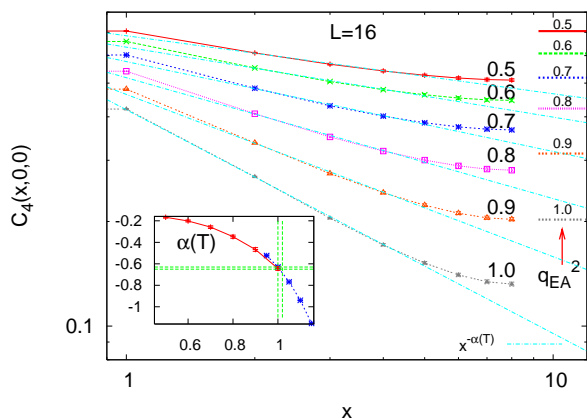


FIG. 24: Behavior of $C_4(x)$ for $L = 16$ and $T = 0.5, 0.6, 0.7, 0.8, 0.9, 1.0$. The interpolation with a simple power-law is also shown. On the right hand side the values of $q_{EA}^2(T)$ are displayed. Inset: behavior of the power α vs. T (full line) compared to the $\alpha(T)$ behavior around criticality for $L = 24$ (dotted line).

pared with the power at criticality, $\alpha = 0.65(1)$.

Decreasing further the temperature we show in Fig. 24 that the behavior is power-law until $x \sim L/4$ is reached. At that point the curves bend upwards as it did at criticality and even at high temperature, cf. Fig. 21. This bending is, however, an artifact due to the contributions induced by the periodic boundary conditions. In Fig. 24, on the right hand side, we show the values of q_{EA}^2 at the same temperatures of the plotted $C_4(x)$. At all temperatures the $C_4(x)$ soon decays below the corresponding value of q_{EA}^2 . For the sizes simulated our data are, thus, not consistent with the observation of a plateau at q_{EA}^2 as predicted by the droplet and TNT theories.

In the present work we have performed Parallel Tempering Monte Carlo numerical simulations in the temperature/crystal field plane of the random 3D Blume-Capel model on a cubic lattice. This is a spin-1 spin glass, whose constituent features try to capture at least one supposed mechanism underlying inverse transitions: the raise of inactive components at low T .

In particular, we have analyzed the second order phase transition carrying out the computation of the critical temperatures and indices by means of parallel tempering simulations in temperature at different values of the chemical potential D . In this analysis we have carefully checked FS effects, identified eventual crossovers from small to large size scaling and neglected data for correspondingly too small sizes. We verified that for different values of D the system is always in the same universality class (as far as a continuous transition occurs) looking, e.g., at different universal scaling functions of ξ_c/L , such as the Binder parameter g , or the quotients of χ_{SG} , ξ_c and g between systems at L and $2L$. The outcome is that at all $D < D_{3c}$ the second order transition belongs to the same universality class of the 3D Edwards-Anderson model for spin-glasses.

We, then, estimated the position of a tricritical point, $D \sim 2.1$, $T \sim 0.5$, beyond which the transition is first order with jump in density and in overlap parameters. This transition is first order in the thermodynamic sense, i.e., latent heat is exchanged and, even though the system is disordered, it is not related to the random first order transition taking place in structural glasses.⁸³ We employed and compared four different methods to infer the critical line from FS data. This observation confirms the claim of Fernandez *et al.*⁵⁶ about the existence of such transitions in quenched disordered short-range finite-dimensional systems. In the present model the first order transition can be seen by means of standard parallel tempering algorithm in the canonical ensemble, simply tuning an external pressure-like parameter.

The first order transition line has the property of displaying inverse freezing, as can be observed from the phase diagram, cf. Figs. 13, 14: the low temperature phase is paramagnetic and the system 'freezes' into a spin-glass phase as T is *increased*. This is at difference with the thermodynamic behavior of the original, ordered, BC model (mean-field or finite dimensional).^{44,51} In presence of quenched disorder, a low temperature paramagnetic phase exists that can acquire a very low density and this is the source of the entropy decrease with respect to the high temperature paramagnetic phase.

Both the inverse freezing transition and its first order nature were not observed in the same model on a hierarchical lattice.⁵⁵

Eventually we present our analysis of the overlap distribution functions and the four-spins correlation functions at criticality and in the glassy phase, at $D = 0$ for T down to $0.5T_c$. From the behavior of site overlap

distribution at zero overlap, $P_L(q_s = 0)$, and from the variance of the link-overlap distribution $P_L(q_l)$ we get evidence in favor of a complex organization of states in the SG phase, displaying features typical of the Replica Symmetry Breaking theory holding for mean-field systems ($d \geq 6$). We cross-checked this observation comparing, with the Kullback-Leibler divergence, the link-overlap distribution with the distribution of a function of the squared site overlap, $q_a \sim A + Bq_s^2$. We carefully analyzed the finite size effects at low temperature finding that for $T < 0.7$ small size fluctuations strongly bias our estimates, yielding *negative* B coefficients of the q_s^2 term, *decreasing* with temperature, unlike any finite size $B(T)$ behavior. In order to have a self-consistent estimate we would need to thermalize at $T \geq 0.7T_c$ systems of size sensitively larger than $L = 16$.

Looking at the position dependence of the four-spins correlation functions we are able to detect, for $T \geq 1.2T_c$, a crossover between a short-distance power-law decay and a long-distance exponential decay and we can identify a length-like parameter ℓ playing the role of the correlation distance, growing as T decreases. As the critical temperature is approached and ℓ becomes similar to the maximum feasible distance in the simulated system ($\sim L/2$),

$C_4(x)$ can be interpolated with a simple power-law. We checked that for sizes $L = 16, 20$ and 24 the exponent of $C_4(x)$ at T_c is equal to $d - 2 + \eta$, where $\eta = -0.36(1)$ is the value obtained from the analysis of the critical properties performed with the quotient method. We also probed the power-law behavior for temperatures down to $0.5T_c$ at distances far away from border, where finite size correction are too strong. Indeed, periodic boundary conditions systematically increase correlations, above all where they are small (or vanishing), i.e., at large distance. We compare the low temperature behavior with the prediction of TNT and droplet theories that $C_4(x)$ should tend to a plateau $C_4 \sim q_{EA}^2$ for large x . Even though we are not able to reach “large x ”, we show that $C_4(x) < q_{EA}^2$ already at small distance.

Acknowledgments

We thank Nihat Berker, Helmut Katzgraber and Federico Ricci-Tersenghi for interesting discussions and exchanges.

-
- * Electronic address: luca.leuzzi@cnr.it
- ¹ G. Tammann, “Kristallisieren und Schmelzen”, Metzger und Wittig, Leipzig (1903).
 - ² J. Wilks, D.S. Betts, *An Introduction to Liquid Helium*, Oxford University Press (USA, 1987).
 - ³ S. Rastogi, G.W.H. Höhne and A. Keller, *Macromolecules* **32**, 8897 (1999).
 - ⁴ A.L. Greer, *Nature* **404**, 134 (2000).
 - ⁵ N.J.L. van Ruth and S. Rastogi, *Macromolecules* **37**, 8191 (2004).
 - ⁶ M. Plazanet *et al.* *J. Chem. Phys.* **121**, 5031 (2004).
 - ⁷ E. Tombari *et al.*, *J. Chem. Phys.* **123**, 051104 (2005).
 - ⁸ M. Plazanet *et al.* *J. Chem. Phys.* **125**, 154504 (2006).
 - ⁹ M. Plazanet *et al.*, *Chem. Phys.* **331**, 35 (2006).
 - ¹⁰ R. Angelini and G. Ruocco, *Phil. Mag.* **87**, 553 (2007).
 - ¹¹ C. Ferrari *et al.*, *J. Chem. Phys.* **126**, 124506 (2007).
 - ¹² R. Angelini, G. Salvi and G. Ruocco, *Phil. Mag.* **88**, 4109 (2008).
 - ¹³ R. Angelini, G. Ruocco, S. De Panfilis, *Phys. Rev. E* **78**, 020502 (2008).
 - ¹⁴ M. Plazanet, M.R. Johnson and H.P. Trommsdorff, *Phys. Rev. E* **79**, 053501 (2009).
 - ¹⁵ R. Angelini, G. Ruocco and S. De Panfilis, *Phys. Rev. E* **79**, 053502 (2009).
 - ¹⁶ C. Chevillard and M.A.V. Axelos, *Colloid. Polym. Sci.* **275**, 537 (1997).
 - ¹⁷ M. Hirrien *et al.*, *Polymer* **39**, 6251 (1998).
 - ¹⁸ A. Haque and E.R. Morris, *Carb. Pol.* **22**, 161 (1993).
 - ¹⁹ N. Avraham *et al.*, *Nature* **411** 451 (2001).
 - ²⁰ M. Greiner *et al.*, *Nature* **415** 39 (2002).
 - ²¹ B. Donnio *et al.*, *Adv. Mater.* **19**, 3534 (2007).
 - ²² B. Donnio *et al.*, *Soft Matter* **6**, 965 (2010).
 - ²³ E. Zaccarelli *et al.*, *Phys. Rev. E* **63**, 031501 (2002).
 - ²⁴ E. Zaccarelli *et al.* *Phys. Rev. E* **66**, 04102 (2004).
 - ²⁵ P.E. Cladis, *Phys. Rev. Lett.* **35**, 48 (1975);
 - ²⁶ P.E. Cladis, *Phys. Rev. Lett.* **39**, 720 (1977);
 - ²⁷ H. Özbek *et al.*, *Ph. Trans.* **75**, 301 (2002);
 - ²⁸ O. Portmann, A. Vaterlaus, and D. Pescia, *Nature* **422**, 701 (2003).
 - ²⁹ A. Srivastava, D. Sa and S. Singh, *Eur. Phys. J. E* **22**, 111 (2007);
 - ³⁰ B. M. Jaffar Ali and A. Kumar, *J. Chem. Phys.* **107**, 8020 (1997).
 - ³¹ D. Bagchi, A.Kumar and R. Menon, *J. Chem. Phys.* **125**, 034511 (2006).
 - ³² H. Verbeek, G.J. Nieuwenhuys, H. Stocker, and J.A. Mydosh, *Phys. Rev. Lett.* **40**, 586 (1978).
 - ³³ Y. Yeshurun, M.B. Salamon, K.V. Rao, and H.S. Chen, *Phys. Rev. Lett.* **45**, 1366 (1980).
 - ³⁴ F.H. Stillinger, P.G. Debenedetti and T.M. Truskett, *J. Phys. Chem. B* **105**, 11809 (2001).
 - ³⁵ F.H Stillinger and P.G. Debenedetti, *Biophys. Chem.* **105**, 211 (2003).
 - ³⁶ M.R. Feeney., P.G. Debenedetti, and F.H. Stillinger, *J. Chem. Phys.* **119** 4582 (2003).
 - ³⁷ N. Schupper and N.M. Shnerb, *Phys. Rev. Lett.* **93** (2004) 037202.
 - ³⁸ N. Schupper and N.M. Shnerb, *Phys. Rev. E*, 72: 046107, 2005.
 - ³⁹ S. Prestipino, *Phys. Rev. E* **75**, 011107 (2007).
 - ⁴⁰ A. Crisanti and L. Leuzzi, *Phys. Rev. Lett.* **95**, 08720170 (2005).
 - ⁴¹ M. Sellitto, *Phys. Rev. B* **73** 180202 (2006).
 - ⁴² M. Sellitto and J. Kurchan, *Phys. Rev. Lett.* **95**, 236001 (2005).
 - ⁴³ A. Allahverdyan and Petrosyan, *Phys. Rev. Lett.* **96**,

- 065701 (2006).
- ⁴⁴ H. W. Capel, *Physica* **32**(1966) 966; M. Blume, *Phys. Rev.* **141** (1966) 517.
- ⁴⁵ S. K. Ghatak, D. Sherrington, *J. Phys. C: Solid State Phys.* **10**, 3149 (1977).
- ⁴⁶ J. Dumas *et al.*, *Phys. Rev. B* **20**, 3913 (1979).
- ⁴⁷ A. Crisanti and L. Leuzzi, *Phys. Rev. Lett.* **89** (2002) 237204.
- ⁴⁸ A. Crisanti and L. Leuzzi, *Phys. Rev. B* **70** (2004) 014409.
- ⁴⁹ L. Leuzzi, *Phil. Mag.* **87**, 543-551 (2006).
- ⁵⁰ M. Blume, V.J. Emery and R.B. Griffiths, *Phys. Rev. A* **4** (1971) 1071.
- ⁵¹ D.M. Saul, M. Wortis and D. Stauffer, *Phys. Rev. B* **9**, 4964 (1974).
- ⁵² A. Nihat Berker and M. Wortis, *Phys. Rev. B* **14**, 4946 (1976).
- ⁵³ A. K. Jain and D. P. Landau, *Phys. Rev. B* **22**, 445 (1980).
- ⁵⁴ M. Hasenbusch, arXiv:1004.4983v1.
- ⁵⁵ V.O. Özçelik and A. N. Berker, *Phys. Rev. E* **78**, 031104 (2008).
- ⁵⁶ L.A. Fernández *et al.*, *Phys. Rev. Lett.* **100**, 057201 (2008).
- ⁵⁷ F.P. Toldin, A. Pelissetto and E. Vicari, *J. Stat. Phys.* **135**, 1039 (2009).
- ⁵⁸ M. Paoluzzi, L. Leuzzi and A. Crisanti, *Phys. Rev. Lett.* , (2010).
- ⁵⁹ K. Hukushima and K. Nemoto, *J. Phys. Soc. Jpn.* **65**, 1604 (1996).
- ⁶⁰ E. Marinari, *Adv. Computer Simul.* **501**, 50 (1998).
- ⁶¹ M. Mézard, G. Parisi and M. A. Virasoro, *Spin glass theory and beyond* (World Scientific, Singapore 1987)
- ⁶² S. Caracciolo *et al.*, *Nucl. Phys. B*403, 475 (1993).
- ⁶³ M. Palassini, S. Caracciolo, *Phys. Rev. Lett.* **82**, 5128 (1999).
- ⁶⁴ W. Kauzmann, *Chem. Rev.* **43**, 219 (1948).
- ⁶⁵ T.L. Hill, *Thermodynamics of Small Systems*, Dover (2002).
- ⁶⁶ R.S. Andrist, H.G. Katzgraber, H. Bombin, M.A. Martin-Delgado, arXiv:1005.0777v1.
- ⁶⁷ E.K. Riedel and F.J. Wegner, *Phys. Rev. Lett.* **29**, 349 (1972).
- ⁶⁸ J. Zinn-Justin, *Quantum Field Theory and Critical Phenomena*, Oxford University Press (Oxford, 1989).
- ⁶⁹ T. Jörg, *Phys. Rev. B* **73**, 224431 (2006).
- ⁷⁰ M. Hasenbusch, A. Pelissetto, E. Vicari, *J. Stat. Mech.* L02001, (2008).
- ⁷¹ H. G. Ballesteros *et al.*, *Phys. Rev. B* **62** (2000) 14237.
- ⁷² E. Marinari, G. Parisi and J. J. Ruiz-Lorenzo *Phys. Rev. B* **58** (1998) 14852.
- ⁷³ F. Belletti *et al.*, *Phys. Rev. Lett.* **101** 157201 (2008).
- ⁷⁴ M. Hasenbusch, F. P. Toldin, A. Pelissetto, and E. Vicari, *Phys. Rev. B* **76**, 094402 (2007); *ibid.* 184202 (2007).
- ⁷⁵ T. Jorg, H. G. Katzgraber, *Phys. Rev. Lett.* **101**, 197205 (2008); *Phys. Rev. B* **77**, 214426 (2008).
- ⁷⁶ D. Sherrington, S. Kirkpatrick, *Phys. Rev. Lett.* **35**, 1792 (1975).
- ⁷⁷ D. S. Fisher, D.A. Huse, *Phys. Rev. Lett.* **56**, 1601 (1986).
- ⁷⁸ F. Krzakala, O.C. Martin, *Phys. Rev. Lett.* **85**, 3013 (2000).
- ⁷⁹ G. Parisi, *Phys. Lett. A* **73** 203-205 (1979), *J. Phys. A* **13**, L115 (1980), *Phys. Rev. Lett.* **50** 1946-1948 (1983).
- ⁸⁰ S. Kullback and R.A. Leibler, *Ann. Math. Stat.* **22**, 79 (1951).
- ⁸¹ P. Contucci *et al.*, *Phys. Rev. Lett.* **99**, 057206 (2007).
- ⁸² L. Leuzzi, G. Parisi, F. Ricci-Tersenghi, J.J. Ruiz-Lorenzo, *Phys. Rev. Lett.* **101**, 107203 (2008).
- ⁸³ L. Leuzzi and T.M. Nieuwenhuizen, *Thermodynamic of the glassy state*, Taylor & Francis (2007).
- ⁸⁴ E.g., setting $S = \sigma n$, with $n = 0, 1$ fast and $\sigma = \pm 1$ slow
- ⁸⁵ We stress that the transition is first order in the thermodynamic sense, with latent heat and is not related to the so-called random first order transition occurring in mean-field models for structural glasses.
- ⁸⁶ In the present work the probability distributions always depend on the size N , or L . In order not to make the notation too heavy, we will explicitate it only when needed.